Ana Catarina Couto Almeida

Licenciada em Química Aplicada

Gold Nanoparticles for Plasmid Delivery

Dissertação para obtenção do Grau de Mestre em Bioquímica

Orientadora: Rita Cabral, Postdoctoral Research Fellow, FCT-UNL

Co-orientador: Pedro M. R. Viana Baptista, Professor Associado com Agregação, FCT-UNL

Júri:

Presidente: Prof. Doutor José Ricardo Ramos Franco Tavares

Arguente: Doutora Inês Isabel Fernandes Gomes

Vogal: Prof. Doutor Pedro M. R. Viana Baptista

FACULDADE DE CIÊNCIAS E TECNOLOGIA
UNIVERSIDADE NOVA DE LISBOA

Setembro 2014

Gold Nanoparticles for Plasmid Delivery

RESUMO

A terapia génica representa uma estratégia ideal para o tratamento de doenças genéticas e adquiridas, como o cancro, e tipicamente envolve a inserção de um gene funcional em células para corrigir uma disfunção celular ou para fornecer uma nova função. Os sistemas de transporte de ácidos nucleicos são baseados em dois modelos: vectores virais e não virais. Os primeiros apresentam uma alta eficiência na entrega do material genético mas a sua maior barreira é a imunogenicidade. Uma vez que os vectores não virais não apresentam imunogenicidade, estes têm sido amplamente estudados. As nanopartículas de ouro têm sido propostas como óptimos sistemas de entrega de material genético, devido ao seu tamanho reduzido, elevado rácio superfície-volume e capacidade de serem funcionalizadas com várias moléculas. No presente trabalho desenvolveu-se uma formulação baseada em nanopartículas de ouro para transporte de um plasmídeo, contendo como gene repórter um gene codificante da proteína verde fluorescente, numa linha celular de cancro colo-rectal. O sistema de entrega resultou da funcionalização de AuNPs de 14 nm com uma múltipla camada de PEG (4300±114 cadeias de PEG/AuNP), aumentando a estabilidade e a biocompatibilidade das AuNPs; amónios quaternários que providenciam cargas positivas que permitem a ligação electroestática do plasmídeo, que é considerado o agente terapêutico que se pretende transportar para dentro das células. O sistema desenvolvido foi caracterizado por espectroscopia de UV-vis, DLS, TEM e análise electroforética em gel de agarose, tendo-se produzindo um sistema com um diâmetro de 113.5 nm. A eficiência da transfecção celular com o sistema desenvolvido foi avaliada por PCR e pela expressão da proteína verde fluorescente (*enhanced green fluorescente protein*, EGFP), através de espectroscopia de fluorescência e microscopia de fluorescência. Verificou-se que a internalização do sistema ocorre após 3h de incubação, no entanto observou-se um nível residual de expressão da proteína. Depois de 24h de incubação, a expressão aumentou 3 vezes em relação às células não transfectadas. O sistema comercial (Lipofectamine) expressou 5 vezes mais EGFP do que o sistema desenvolvido AuNP@PEG@R_4N^+@pEGFP. Esta diferença poderá estar relacionada com a menor translocação para o núcleo.

Termos chave: nanopartículas de ouro, bioconjugação, nanotransportador, terapia génica, DNA plasmídico, cancro

ABSTRACT

Gene therapy presents an ideal strategy for the treatment of genetic as well as acquired diseases, such as cancer and typically involves the insertion of a functioning gene into cells to correct a cellular dysfunction or to provide a new cellular function. Gene delivery vectors are based in two models: viral and non-viral. Viral vectors have high transfection efficiency but their major barrier is immunogenicity. Since the non-viral vectors have no immunogenicity, these have been widely studied. Gold nanoparticles have been proposed as optimal delivery systems of genetic material, due their small size, high surface-to-volume ratio and the ability to be functionalized with multiple molecules. In the present work, an AuNP-based formulation was developed to deliver a plasmid in a colorectal cancer cell line, containing as reporter gene the gene encoding to EGFP. The delivery system resulted from the functionalization of 14 nm AuNP with a PEG layer (4300±114 PEG chains/AuNP), which increases stability and biocompatibility of AuNPs; quaternary ammonium groups which provide positive charges that allow electrostatic binding of plasmid, which is considered the therapeutic agent to be transported into cells. The system developed was characterized by UV-vis spectroscopy, DLS, TEM and by electrophoretic mobility, yielding a formulation with 113.5 nm.Transfection efficiency of the formulation developed was evaluated through PCR and through EGFP expression by fluorescence microscopy and fluorescence spectroscopy. The internalization was observed 3h post transfection; however a low level of EGFP expression was achieved. After 24h of incubation, EGFP expression increases just 3 times compared to non-transfected cells. The commercial system (Lipofectamine) expressed EGFP 5 times more than the system developed AuNP@PEG@R_4N^+@pEGFP. This difference could be related to lower translocation to the nucleus.

Keywords: gold nanoparticles, bioconjugation, nanocarrier, gene therapy, plasmid DNA, cancer

TABLE OF CONTENTS

FIGURE INDEX

TABLE INDEX

ABBREVIATIONS

AuNPs	Gold Nanoparticles
cDNA	complementary DNA (DNA synthesized from mRNA template)
DEPC	Diethylpyrocarbonate
DLS	Dynamic Light Scattering
DMEM	Dulbecco's Modified Eagle Medium
dNTPs	Deoxyribonucleotide Triphosphate
dsDNA	double-stranded DNA
DTNB	5,5'-dithio-bis(2-nitrobenzoic) acid
EDC	1-Ethyl-3-(3-dimethylaminopropyl) carbodiimide
EGFP	Enhanced Green Fluorescent Protein
EGFR	Epidermal Growth Factor Receptor
FBS	Fetal bovine serum
FTO	Fat mass obesity associated gene
HCT-16	Human Colorectal Carcinome
LSPR	Localized surface plasmon resonance
MDR	Multiple drug resistance
MES	2-(*N*-morpholino)ethanesulfonic acid
MTS	(3-(4,5-dimethylthiazol-2-yl)-5-(3-carboxymethoxyphenyl)-2-(4-sulfophenyl)-2H-tetrazolium)
MW	Molecular weight
PBS	Phosphate Buffer Saline
pDNA	Plasmid DNA
PEG	Poly (ethylene glycol)
PMS	Phenazinemethosulfate
rpm	Revolutions per minute
R_4N^+	Quaternary ammonium
SDS	Sodium Dodecyl Sulfate
siRNA	Small interfering RNA
Sulfo-NHS	N-hydroxysulfosuccinimide
TEM	Transmission electron microscopy
ε	Molar extinction coefficient

1. INTRODUCTION

1.1 CANCER: AN OVERVIEW

Cancer is one of the leading causes of mortality in the modern world, with more than 10 million new cases every year. According to GLOBOCAN 2012, the three types of cancer with the highest incidence at a global level are the breast, lung and colorectal cancers, while the highest mortality rate is associated with lung, colorectal and stomach cancers [GLOBOCAN, 2012].
Cancer is defined as a multifactorial disease characterized by uncontrolled growth and spread of abnormal cells. Behind the origin of cancer are factors that can be internal, such as inherited mutations, hormones, immune conditions, and mutations that occur from metabolism and external factors like tobacco, infectious organisms, chemicals, and radiation (Cancer Facts & Figures 2014).

The main characteristic common to different types of cancer are proliferative signaling, evasion of growth suppressors, resistance to cell death, replicative immortality, angiogenesis, invasion and metastasis (Hanahan & Weinberg 2011).

1.1.1 CURRENT NEEDS

The potential to provide new targets and strategies for cancer therapy lies in understanding cancer biology. A huge amount of research has already been carried out, resulting in a number of available treatments. Currently, the most common therapies include surgery, radiation, chemotherapy, hormone therapy, biological therapy, and targeted therapy (Cancer Facts & Figures 2014).

However, these available treatments are limited because the agents used do not differentiate between cancerous and normal cells, causing toxicity to healthy cells, severe side effects and eventually multiple drug resistance. Thus, the main goal in cancer treatment is to develop a therapeutic system that takes advantage of the potency of therapeutic agents by more effectively targeting them to tumor tissues (Liu et al. 2007, Nazir et al. 2014)

1.2 GENE THERAPY

Many human diseases result from genetic mutations, including deletions and insertions, which lead to disorders in metabolic pathways, ligand/receptor function, cell cycle regulation, cell skeleton or extra-cellular protein structure and function. Generally, gene therapy approaches are based on the employment of genetically engineered vectors that promote the transfer of nucleic acids into cells in order to regulate, repair, replace, add or delete a genetic sequence (Cevher et al. 2012, Gascón et al. 2013, Kaliberov & Buchsbaum 2012, Liu & Zhang 2011).

An ideal gene delivery system should be stable, biocompatible, nontoxic, present lack of immunogenicity, capable of highly efficient transport of exogenous genetic material into their target sites, resistant to premature degradation and capable of modulation of gene expression for a desired period of time (Jones et al. 2013, Liu & Zhang 2011).
Nucleic acids have been explored to treat various diseases, such as cancer, genetic disorders, infections and cardiovascular diseases. Thus, gene therapy involves the use of nucleic acid as therapeutics agents, such as plasmid DNA (pDNA), oligonucleotides, small interfering RNA (siRNA), aptamers, Ribozymes or DNAzymes.

Plasmid vectors are high molecular weight, double-stranded DNA constructs containing transgenes, which encode specific proteins. In the early stages of development, plasmid-based gene therapy can be employed to correct inheritable disorders resulting from a single gene defect. Gene therapy using plasmid DNA is based on the introduction of the pDNA, encoding a therapeutic gene sequence, into the nucleus of the target cells to express functional proteins, through transcription and translation (Liang & Lam 2012, Pushpendra et al. 2012). The mechanism of action of plasmid DNA involves the entry of plasmid molecules into the nucleus after entering the cytoplasm. The entry of plasmid molecules into the nucleus through the nuclear pore complexes is an extremely challenging and difficult process that controls the efficiency of gene expression (Patil et al. 2005, Pushpendra et al. 2012). Gene expression is also controlled by regulatory signals such as the promoter and enhancer sequences. Promoter sequences initiate the transcription process by acting as a recognition site for the RNA polymerase. Higher efficiency can be obtained by engineering the plasmid with strong tissue- or tumor-specific promoters (Elsabahy et al. 2011).

Another approach for induction of transgenes is suicide gene therapy. This method involves the stable transfection of chemosensitization genes in tumor cells, which upon gene expression convert a separately administered, nontoxic pro-drug into a chemotoxic drug. Since only the transfected tumor cells are capable of this intracellular conversion, only these cells are susceptible to the chemotoxic entity (Patil et al. 2005).

Oligonucleotides are another type of nucleic acid that can be used as therapeutic agent. Oligonucleotides are short single-stranded segments of DNA (12 – 28 bases) that can selectively inhibit the expression of a single gene. Two approaches are used with oligonucleotides, antisense and antigene. The first involves the interaction of oligonucleotides with mRNA, forming a duplex, inhibiting their translation or processing and consequently inhibiting protein expression. The antigene approach requires the entry of oligonucleotides into the nucleus and the insertion between double strands of genomic DNA to form a triple-helix structure, preventing the transcription and subsequent translation of the gene.

Another gene therapy approach involves the delivery of small interfering RNA (siRNA). This is used as posttranscriptional mechanism of gene silencing. Typically, these are short double-stranded RNA segments with 21–23 nucleotides, namely the guide strand and passenger strand, the former of which is complementary to the target mRNA sequence of the gene whose translation is to be blocked. The mechanism of action involves the incorporation of the siRNA guide strand into RNA-induced silencing complexes (RISCs), which bind to the mRNA of interest and stimulate mRNA degradation mechanisms, such as nuclease activity, that lead to silencing of the particular gene. This approach using siRNAs is more promising than antisense oligonucleotides due their high degree of specificity to mRNAs. Furthermore, this technology has a more rapid development that oligonucleotides or plasmid DNA, because siRNAs does not have to enter the nucleus for their activity and require less refined delivery systems (Patil et al. 2005, Pushpendra et al. 2012).

Aptamers are another class of nucleic acids used in gene therapy. These are single stranded oligonucleotides (RNA or DNA) that recognize their targets on the basis of shape complementarity. The mechanisms of action are different from other oligonucleotides because, while some oligonucleotide therapies interfere with the translational machinery, aptamers target proteins directly and bind to them, altering their function. Their behavior is similar to antibodies and is preferred over antibodies in protein inhibition due their specificity and nonimmunogenicity (Prasad & Roy 2008, Pushpendra et al. 2012)

The last type of gene therapy agents are ribozymes. These are RNA enzymes that are capable of sequence specific cleavage of mRNA molecules, resulting in selective inhibition of expression of deleterious genes. In their mechanism of action, a ribozyme binds specifically to an mRNA strand and cleaves it, preventing its translation. After cleavage, the enzyme is released and is ready for binding and destroying another mRNA molecule, leading to highly specific knockdown of the target genes. The presence of the RNA backbone in ribozymes makes them biologically unstable in vivo because these are easy targets for degradation by RNases (Prasad & Roy 2008, Pushpendra et al. 2012).

Another type of nucleic acid enzymes are DNAzymes. They are analogs of ribozymes with greater biological stability because the RNA backbone chemistry is replaced by the DNA motifs that confer improved biological stability (Patil et al. 2005).

The focus of this work is the delivery of plasmid DNA. Until now, there are no plasmid DNA based therapeutic products approved by the FDA due the lack of an efficient and safe delivery system, which limits the clinical application of nucleic acids (Liang & Lam 2012). However, there are two methods that have been used in gene therapy clinical trials using non-viral vectors: one involves the injection of naked plasmid DNA into a tissue. This has been used in ~14% of

approved clinical trials. The other method is transfection of plasmid DNA using liposomes and has been used in ~9% of approved trials (Cotrim & Baum 2008).

1.2.1 GENE DELIVERY SYSTEMS

Gene delivery systems can be divided in viral and non-viral systems. Viral vectors consist of viruses that are genetically engineered to be replication-deficient. They are the most effective but their immunogenicity, oncogenicity, small size of the DNA they can transport and the difficult optimization in large-scale production limit their applications. Non-viral have gain more attention due their favorable properties, including lack of immunogenicity, low toxicity, potential for tissue specificity, large gene insert size and they are low cost and more reproducible. The main limitation of non-viral systems is their low transfection efficiency. Currently, viral vector has dominated the clinical trials in gene therapy for its relatively high delivery efficiency, as show in Figure 1.1, standing out the adenovirus with 23.4%, the retrovirus with 19.2% and plasmid DNA with 17.8% (Gascón et al. 2013, Kaliberov & Buchsbaum 2012, Liu & Zhang 2011).

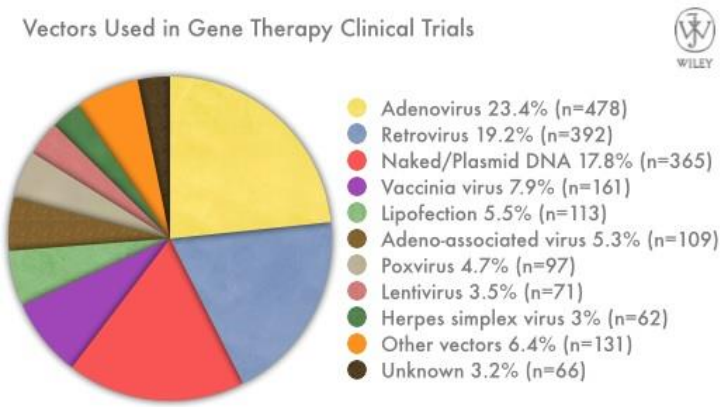

Figure 1.1 - Current gene delivery vectors in clinical trials (http://www.wiley.com//legacy/wileychi/genmed/clinical/).

Non-viral gene delivery systems were developed as an alternative to viral-based systems. They can be divided into physical methods where a physical force is applied to increase permeability of the cell membrane and chemical methods that use natural or synthetic carriers to delivery genes into the cell (Cevher et al. 2012).

1.2.1.1 NON-VIRAL GENE DELIVERY SYSTEMS

Nucleic acids are incapable of crossing the plasma membrane due their large size and hydrophilic nature, due to their negatively charged phosphate groups, and they are very susceptible to nuclease degradation. As such, is necessary to develop delivery systems and physical methods that facilitate gene transfer to target cells without degradation of the delivered

gene, promote cellular uptake, release nucleic acids into the cytoplasm and promote nuclear entry (for pDNA delivery). Physical and chemical methods can help delivery systems to cross plasma membrane in *in vitro* and *ex vivo* applications. Numerous non-viral delivery systems have been developed and widely studied during the past years, as show in Table 1.1 (Chou et al. 2011, Liang & Lam 2012).

The most well studied non-viral gene delivery systems are cationic polymers and cationic lipids.

Table 1.1 – Current non-viral delivery systems (Al-Dosari & Gao 2009, Cevher et al. 2012, Gascón et al. 2013, Wang et al. 2013).

	Method	Brief description	Advantages	Limitations
Chemical methods	Cationic Polymers	Condense DNA into small particles protecting it from degradation	Easy to be prepared and chemically modified, low cost, highly effective	Toxicity. Some polymers are non-biodegradable.
	Cationic Lipids	Condense DNA into cationic particles protecting it from degradation	Easy to be prepared, low cost, highly effective *in vitro*	Toxicity, low efficiency *in vivo*
	Inorganic nanoparticles	Nanostructures varying in size, shape and porosity, which can be engineered	Easily prepared and surface-functionalized, low toxicity and good storage stability	*in vivo* applications are limited by the lack of extensive studies
Physical methods	Needle injection	Localized injection of naked DNA into muscle or skin	Simple and safe	Low efficiency
	Gene Gun	DNA-coated gold particles are propelled against cells	Allows delivering precise DNA doses; safe	Tissue damage
	Electroporation	Use an electric field to alter the cell permeability	Effective, reproducible, able to transfer large size DNA	Inaccessible to internal organ; DNA stability is influenced by high voltage
	Sonoporation	Use ultrasounds to permeabilize the cell membrane	Non evasive, site-specific	Low efficiency
	Photoporation	Use a single laser pulse to alter the cell permeability	Selectivity; high transfection	Further studies are needed to become applicable
	Magnetofection	Use a magnetic field to promote DNA transfection which is complexed with magnetic nanoparticles	Non-invasive; Low-dose requirements and allow magnetic targeting	Toxicity
	Hydrodynamic gene delivery	Employs the high pressure as a driving force for gene transfer	Highly effective, reproducible, simple	Large injection volume restricts its clinical application

1.2.2 BARRIERS FOR NON-VIRAL GENE DELIVERY METHODS

The inefficiency of gene delivery primarily results from the inability of the vectors to surpass the inumerous barriers encountered from the site of administration to localization in the cell nucleus. Generally, the barriers can be divided into extracellular and intracellular. Extracellular barriers are characterized by vector stability, blood components and opsnization and last endothelial barriers, such as blood brain barrier, vitreous humor, respiratory mucus.

A prerequisite for efficient gene transfer is the delivery of nucleic acids from outside the cell to the nucleus. However, for gene delivery in particular, intracellular barriers represent an extra concern when designing the formulation. There are four major intracellular barriers:

1. Cellular binding
2. Cellular uptake
3. Endosomal escape
4. Nuclear entry

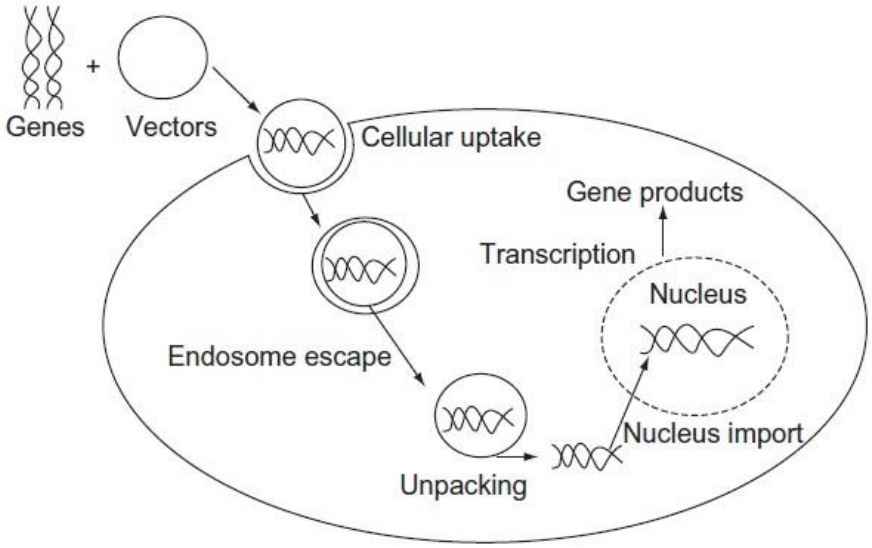

Figure 1.2 – Barriers and intracellular trafficking of plasmid DNA. The first step is the complexation of DNA with the delivery vector; DNA can be internalized via receptor-mediated pathways, including endocytosis, or by receptor-independent mechanisms. Once inside the cells the vector needs to escape from the endosome, cross the cytoplasm, the DNA needs dissociate from the vector and reach into the nucleus where it can be transcribed (Liu & Zhang 2011).

As mentioned above, the first barrier is crossing the cell membrane, a lipid dynamic bilayer that regulates the transportation of ions, nutrients, and wastes. This step is considered one of the most critical for efficient DNA transfection. Non-viral vectors can interact with the cell membrane by electrophilic attraction between the cationic vectors and the highly anionic cell membrane surface proteoglycans. In order to improve transfection efficiency, non-viral vectors can be conjugated with a specific ligand allowing delivery to a specific cell type. Peptides, proteins,

carbohydrates and small molecules have been used to induce target cell-specific internalization (Al-Dosari & Gao 2009, Gascón et al. 2013, Liu & Zhang 2011).

Commonly, internalization is achieved by endocytosis. During this process, some part of the plasma membrane surrounds the vector and engulfs into a vesicle that then pinches off from the cell membrane, enters the cytosol and cross into the cell to its intracellular target. Endocytosis is divided into phagocytosis (the uptake of large particles) and pinocytosis (the uptake of fluids and solutes). While phagocytosis is restricted to specialized phagocytes such as macrophages, neutrophils and monocytes, pinocytosis occurs in all types of cells. Pinocytosis is divided in four classes: (i) clathrin-mediated endocytosis; (ii) caveolae-mediated endocytosis; (iii) macropinocytosis; (iv) clathrin- and caveolae- independent endocytosis (El-Sayed & Harashima 2013, Khalil et al. 2006, Liu & Zhang 2011).

The transfection efficiency of nucleic acid delivery systems is correlated not only with the level of cellular uptake but also with their ability to escape from endosomal compartments. Once inside the cells, delivery vectors tend to be trapped in the early endosome, where the pH drops from neutral to around pH 6 and then traffic through the cell (Liang & Lam 2012, Liu & Zhang 2011).The evolution of endosomes into late endosomes and lysosomes (the main degradative compartments in the cell) is characterized by rapid acidification from pH 6 to 4 within the vesicle and recruitment of degradative enzymes into the vesicle to digest vesicular content. Therefore, gene escape from the endolysosomal network becomes a very important limiting step in achieving an effective gene therapy (Chou et al. 2011, Liang & Lam 2012).

Several approaches have been developed to promote early endosomal escape of non-viral gene delivery systems and many hypotheses have been suggested to explain these processes. One of the hypotheses, proposed for cationic polymers and dendrimers, is the proton-sponge effect. However, this hypothesis is also applied to nanoparticles, since these can be coated with high pH buffering capability peptides that undergo structural deformation under acidic pH to disrupt the vesicle membrane. During the maturation of endosomes, the membrane-bound ATPase proton pumps actively translocate protons from the cytosol into the endosomes, leading to the acidification of endosomal compartments (Figure 1.3). At this stage, polymers with the ‘proton sponge’ property will become protonated and resist the acidification of endosomes. As a result, more protons will be continuously pumped into the endosomes with the attempt to lower the pH. The proton pumping action is followed by passive entry of chloride ions, increasing ionic concentration and leading to water influx. Eventually the osmotic pressure causes swelling and rupture of endosomes, releasing their entrapped material (Liang & Lam 2012).

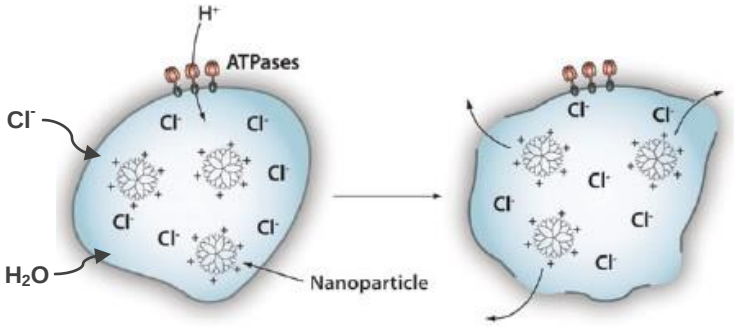

Figure 1.3 – Endosomal escape by the ‘‘proton-sponge effect’’. During maturation of endosome, pH decrease from 6 to 4. The protons pumps pump H^+ ions inside the endosome. These protons are sequestered by the entrapped material, sustaining the action of the proton pump. An influx of Cl- ions and water accompanies the influx of protons and this causes swelling and the rupture of endosome, allowing entrapped material to escape (adapted from Chou et al. 2011).

Another mechanism for endosomal escape is the destabilization of the endosomal membrane. Once inside the endosomes, cationic lipoplexes interact electrostatically with negatively charged lipids of the endosomal membrane. Consequently, anionic lipids of the endosomal membrane diffuse into the lipoplexes and form charge-neutralized ion pairs with the cationic lipids of the lipoplexes. As a result, the nucleic acids are moved from the lipoplexes, allowing the nucleic acids to be released into the cytoplasm(Liang & Lam 2012, Liu & Zhang 2011).

Pore formation is another hypothesis proposed to explain the endosomal escape of peptide-based nucleic acid delivery systems. This mechanism is based on the fact that some peptides have high affinity for the rim of the pore. Pore forming peptides induce bending of the membrane and contiguity of the bilayer leaflets, thus opening a pore in the membrane and facilitating release of endosomal contents (Medina-Kauwe et al. 2005, Varkouhi et al. 2011).

The last hypothesis proposed to endosomal escape is the photochemical disruption of the endosomal membrane. Photochemical internalization (PCI) is a light-directed delivery method that utilizes photosensitizers to facilitate the transport of membrane impermeable macromolecules from endocytic vesicles into cytoplasm. Once confined in the endosome and exposed to light, these photosensitizers induce the formation of reactive oxygen species, mainly singlet oxygen, leading to the rupture of endosome membrane, whereas the contents of the organelles remain intact. As a result, entrapped material can be released into the cytosol (Liang & Lam 2012, Varkouhi et al. 2011).

The last barrier that is critical for successful plasmid expression is the nuclear entry, because plasmids cannot be expressed unless they cross the nuclear envelope and enter the nucleus. The mechanisms of DNA nuclear translocation and whether the DNA stays associated with the delivery system are not yet well understood but this appears to depend on the type of delivery vehicle. However, there are three known pathways for DNA transport to the nucleus (Liu & Zhang 2011):

1. During the cell division stage, in which the nuclear membrane is temporarily broken down, allowing nuclear uptake of plasmid DNA.
2. By passive transport through nuclear pores. The nuclear envelope is interrupted by large protein structures called nuclear pore complexes (NPC) which allow free diffusion of molecules less than 9 nm, or with MW less than 60 kDa or nucleic acids of up to 300 bp. This route is not applicable to plasmids since gene delivery vectors are much larger than 9 nm.
3. By active transport through nuclear pore complexes for particles less than 25 nm. This active transport is regulated by specific nuclear import and export systems such as nuclear localization signal (NLS) peptides (Al-Dosari & Gao 2009, Liu & Zhang 2011, Vaughan et al. 2006).

After the plasmid enters the nucleus, a low level expression can occur and may be explained by the fact that, in most cases, the plasmid stays in the nucleus as an episomal DNA molecule without substantial chance to integrate into the host genome. During cell division these episomes do not replicate and will eventually be diluted away as the population of dividing cells grows (Al-Dosari & Gao 2009).

1.3 NANOBIOTECHNOLOGY

Nanotechnology is a multidisciplinary field that brings together diverse fields of research and development such as engineering, biology, physics and chemistry (Baptista 2009) .Formally, nanotechnology can be defined as the design, development and application of structures, devices and systems by controlling shape and size at the nanometer scale, i.e., at the level of atoms, molecules, and supramolecular structures. The nanometer scale is interesting in biological systems given the inherent nanoscale of functional components of living cells. So, it was inevitable that nanotechnology would be applied to biotechnology. Thus, the fusion between nanotechnology and biotechnology has created a new field of research – Nanobiotechnology (Eustis & el-Sayed 2006, Jain 2008, Khalel et al. 2010).

Nanobiotechnology can be considered a field that concerns the utilization of biological systems, such as cells, cellular components, nucleic acids, and proteins, to formulate functional nanostructures comprised of organic and inorganic materials, such as gold nanoparticles, magnetic nanoparticles, quantum dots, dendrimers, fullerenes, etc (Ladj et al. 2013, Nazir et al. 2014). But it also concerns the development and application of instruments, originally designed to generate and manipulate nanostructured materials, to study fundamental biological processes and structures (Niemeyer & Mirkin 2004). Nanobiotechnology comprises all areas of physical and chemical sciences, biological sciences, health sciences and other interdisciplinary fields. In particular, bionanotechnology has had an increasing impact within the healthcare field. A number of clinical applications, such as disease diagnosis, target-specific drug delivery, gene

delivery and molecular imaging are being investigated at present (Fakruddin et al. 2012, Liang et al. 2012)

Several approaches have been considered for the development of nanotheranostic techniques. However, nanoparticles (size range 1-100 nm) are one of the most common approaches, due their high surface-to-volume ratio, quantum size effect and electrodynamics interactions. Between these, gold nanoparticles are the most extensively studied nanomaterials and have led to the development of innumerous techniques and methods for molecular diagnostics, imaging, drug delivery, gene therapy, photothermal therapy and cell cycle regulation (Dreaden et al. 2011, Liang et al. 2012).

1.3.1 GOLD NANOPARTICLES

Gold nanoparticles have been used since ancient times due to their optical properties, in particular for staining glass. Systematic investigations on gold nanoparticles go back to the days of Faraday, when he reported the formation of deep red solutions upon reduction of chloroaurate ($AuCl_4^-$) with white phosphorous. However their use in biological applications happened only in the last decade (Haiss et al. 2007, Sperling et al. 2008)

Gold nanoparticles, also known as colloidal gold, are a suspension of sub-micrometer-sized gold metal particle in a fluid and can be obtained with diameters between 3 and 200 nm. AuNPs have gained increasing interest because they exhibit features which are fundamentally different from all other nanostructures. Their simple and fast preparation, controllable morphology and size dispersion and shapes, extraordinary optical and electronic properties, easy surface functionalization, high stability and biological compatibility, and the efficient conversion of light into heat, make them powerful agents within the anti-cancer nanotechnology filed of research (Huang et al. 2007, Sperling et al. 2008)

Gold nanoparticles represent a versatile, potent, selective, and highly multi-functional anti-cancer technology. Due their small size, gold nanoparticles can easily interact with biomolecules both at surface and inside cells, improving signals and providing target specificity for diagnostics and therapeutics (Conde et al. 2012b)

1.3.1.1 Optical properties

Once matter is exposed to light, several processes can occur and light can be absorbed, scattered at the same frequency as the incoming light (Rayleigh scattering), absorbed and re-emitted (fluorescence) or enhanced, enhancing any spectroscopic signals from the molecules at the material surface (surface-enhanced Raman scattering). In the case of gold nanoparticles, all these processes are enhanced strongly owing to the unique interaction of light with the free

electrons on their surface (Huang et al. 2007). Gold nanoparticles have shown a range of biological and biomedical applications, due to their electrical, chemical and mainly to their strongly enhanced optical properties (Huang et al. 2007, Khan et al. 2013). The optical properties of gold nanoparticles are significant because absorption and emission can occur within the visible range of light (El-Sayed 2001).

For biomolecular detection, an important feature of gold nanoparticles is the surface plasmon resonance (SPR). The SPR is the collective oscillation of the free electrons within the conduction band. The oscillation frequency is usually in the visible region giving rise to the strong SPR absorption. The SPR is very sensitive to the composition, size, shape, inter-particle distance and environment (dielectric properties) of the gold nanoparticles (Boisselier & Astruc 2009, Conde et al. 2014a) .For gold nanospheres, 14 nm diameter nanoparticles, this resonance occurs in the visible spectral region at approximately 520 nm, which is the origin of the red color of these nanoparticles in solution (Eustis & el-Sayed 2006, Huang et al. 2007). The plasmon resonance frequency is changed when the average distance between gold nanoparticles is reduced (so that they form small aggregates), and as a consequence, the colloidal solution changes from red to dark blue and the SPR band changes to major wavelengths (Sperling et al. 2008).

1.3.2 GOLD NANOPARTICLES SYNTHESIS

The first scientific report describing the production of colloidal gold nanoparticles came in 1857 when Michael Faraday found that the ‘‘fine particles’’ formed from the aqueous reduction of gold chloride by phosphorus could be stabilized by the addition of carbon disulfide, resulting in a ‘‘beautiful ruby fluid’ (Faraday 1857). Currently, the methods to obtain gold nanoparticles follow a similar strategy in which a gold salt is reduced in the presence of a reducing agent and a surface capping agent, the latter preventing aggregation of the particles by electrostatic repulsion (Dreaden et al. 2012). In 1951, *Turkevich* provided the first structural study of gold nanoparticles formed under varying synthetic conditions (Turkevich et al. 1954). Later, in 1973, *Frens* improved the Turkevich’s method, producing monodisperse spherical gold nanoparticles with different diameters (Frens 1973).

The most common method for the synthesis of colloidal gold nanoparticles involve the chemical reduction of Au (III) to Au (0) by citrate in water. In the citrate reduction method, hydrogen tetrachloroaurate (HAuCl4) is reduced by sodium citrate. The particles are stabilized by citrate ions bound to the surface of the nanoparticles, resulting in negatively charged nanoparticles that repel each other by electrostatic repulsion. The sizes of the resulting gold nanoparticles are dependent of the citrate/Au ratio with larger ratios leading to smaller diameters (Dreaden et al. 2011).

The second popular method using such sulfur coordination for gold nanoparticles stabilizations the Shiffrin–Brust biphasic synthesis using HAuCl4, a thiol, tetraoctylammonium bromide and NaBH4 in water–toluene yielding thiolate-AuNPs (Brust et al. 1994). Other methods to synthesize gold nanoparticles have also been reported. A multiplicity of other sulfur ligands such as xanthates, dithiocarbamates, disulfides, di- and trithiols, and resorcinarenes, polythioethers have been used to stabilize and synthesize AuNPs upon reaction with a Au (III) in the presence of a reductant. However, generally these ligands are not used for medical applications (Llevot & Astruc 2012).

1.3.3 GOLD NANOPARTICLES FUNCIONALIZATION

The gold nanoparticle surface represents one of the most stable and easily functionalized platforms for molecular conjugation. Functionalization of nanoparticles is necessary for their stability, functionality, specificity and biocompatibility. The main goal in functionalization is to maintain the properties of the gold nanoparticles and the bound molecules. The molecules should be stable and able to retain their features and gold nanoparticles should be able to retain their unique properties (Delong et al. 2010, Dreaden et al. 2011, 2012).

In the design of biomedical gold nanoparticle conjugates, stability is an important feature because the physiological environments exhibit high ionic and serum concentrations which can disrupt and diminish the stabilizing capacity of many nanoparticle ligands. Thus, electrostatic repulsion alone is often insufficient to prevent particle aggregation. Poly(ethylene glycol) (PEG) is the most common surface ligand used to stabilize biomedical nanoparticles and can be attached to gold surface by a thiol linker. Pegylation not only increases stability and hydrophilicity, but also decreases immunogenic response from the nanoparticles, as well as their recognition by the reticuloendothelial system (RES) by minimizing adsorption of proteins and molecules which initiate phagocytic uptake (Dreaden et al. 2011, 2012).

The gold nanoparticles surface can be functionalized with a variety of (bio) molecules such as DNA/RNA, oligonucleotides (siRNA, ssDNA), peptides, proteins, antibodies, polymers, drugs, cell surface receptors, and tumoral markers (Figure 1.4). If the (bio) molecule has a functional group which can bind to the gold surface, like thiols or specific peptide sequences, these can replace some of the original stabilizer molecules. Alternatively, (bio) molecules can be attached to the shell of stabilizer molecules around the gold nanoparticles by bioconjugate chemistry. The functional molecular linkers utilized for attachment of (bio) molecules to the gold surface generally include thiolates, dithiolates, amines, carboxylates, cyanides, isothiocyanates, phosphines, etc (Dreaden et al. 2011, Sperling et al. 2008, Tiwari et al. 2011).

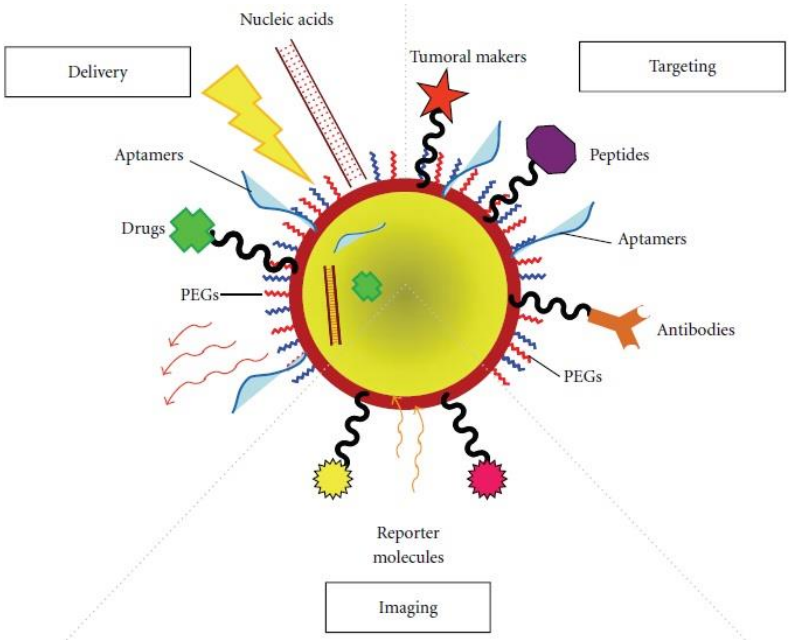

Figure 1.4 – Schematic representation of a multifunctional nanoparticle. These innovative nanoparticles comprise nucleic acids, aptamers and anti-cancer drugs used for delivery to the target tissue. Tumoral markers, peptides, PEGs and antibodies can be used to improve nanocarrier circulation, effectiveness and selectivity. Reporter molecules attached to the particle surface can be employed as tracking and/or contrast agents (Conde et al. 2012b).

The most common method to attach biomolecules by bioconjugate chemistry is the covalent linkage of amino groups on the biological molecules with carboxyl groups at the free ends of stabilizer molecules (e.g. thiolated PEG) by using 1-ethyl-3-(3-dimethylaminopropyl) carbodiimide HCl-mediated reaction, as shown in Figure 1.5 (Sperling et al. 2008).

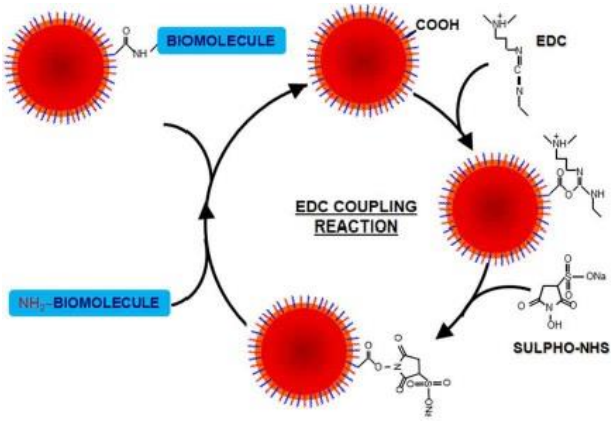

Figure 1.5 – EDC coupling reaction scheme. EDC is a zero-length crosslinking agent used to couple carboxyl groups to primary amines. In the presence of sulfo-NHS, EDC can be used to convert carboxyl groups to amine-reactive sulfo-NHS esters. The addition of sulfo-NHS stabilizes the amine-reactive intermediate by converting it to an amine-reactive Sulfo-NHS ester, thus increasing the efficiency of EDC-mediated coupling reactions (Conde et al. 2014a).

The (bio) molecules can also be attached to gold nanoparticles by electrostatic adsorption of negatively charged (bio) molecules to positively charged nanoparticles or vice versa and by non-covalent binding, affinity-based receptor-ligand systems (Sperling & Parak 2010).

1.3.4 GOLD NANOPARTICLES FOR DELIVERY APPLICATIONS

Facing the problems inherent to current cancer treatments, nanotechnology has the potential to revolutionize cancer diagnosis and therapy. Thus, targeting of nanoparticles takes advantage of the inherent size of nanoparticles and the characteristic features of tumor biology, such as enhanced permeability and retention (EPR) effect, that allow nanoparticles to accumulate in the tumor, in conjunction with extracellular acidic pH, hypoxia, angiogenesis (development of a network of new blood vessels) and abnormal lymphatics. As a consequence of the EPR effect, the passive transport of macromolecules leads to their accumulation in tumors at considerably higher concentrations than in normal tissues, mostly 10-100 times higher within 1-2 days (Nazir et al. 2014).

Nanotechnology had the main challenge to provide new cancer nanotherapies through the development of therapeutic nanocarriers that have the potential to provide effective therapies with minimal side effects and high specificity (Peer et al. 2007).

Since nanocarriers encounter numerous barriers in route to their target, it is necessary to combine the rational design of nanocarriers with the fundamental understanding of tumour biology. Therefore, the developed nanocarriers should be capable of circulating in the blood stream undetected by the immune system, exhibit high differential uptake efficiency in the target cells over normal cells, be soluble or colloidal under aqueous conditions for increased effectiveness and have an extended circulating half-life (Peer et al. 2007).

Nanocarriers can offer many advantages over free therapeutic agents. They can protect the therapeutic agent from premature degradation and prematurely interacting with the biological environment, can improve intracellular penetration and control the pharmacokinetic distribution. At last, nanocarriers take advantage of EPR (enhanced permeability and retention) effect which increase absorption of the agent into a selected tissue (Peer et al. 2007).

1.3.4.1 CELLULAR UPTAKE AND TOXICITY OF GOLD NANOPARTICLES

Gold nanoparticle size, colloidal stability and biocompatibility are the most exploited properties for delivery applications. The main goal of the incorporation of gold nanoparticles into the cells is to transfer molecules which are adsorbed on the surface of the gold nanoparticles. Targeting cancer cells is possible by conjugating gold nanoparticles with ligands specific to receptors

which are overexpressed on the surface of cancer cells but that are less present on healthy cells (Sperling et al. 2008).

Understanding the mechanism of gold nanoparticle uptake by cells is important for intracellular drug and gene delivery. Most of the nanoparticle conjugates are capable of exhibiting some degree of intracellular incorporation. To internalize nanoparticles, cells utilize phagocytosis, macropinocytosis and receptor mediated endocytosis (RME) pathways including caveolae-mediated, clathrin-mediated, and caveolae/clathrin independent endocytosis. For gold nanoparticles, most of the studies reported nanoparticles with dimensions of less than 100 nm and endocytosis has been proposed as the primary mechanism of cellular internalization. The size of nanoparticles was found to play a critical role in rate and extent of cellular uptake. In the work reported by Chithrani et al, it was found that 50 nm transferrin-coated gold nanoparticles were taken up by mammalian cells at higher rates and extents compared to smaller and larger sizes in the range of 10–100 nm (Chithrani et al. 2006). However the optimal particle size for intracellular uptake depends on the cell size, type, receptor density, metabolic activity, etc., as well as the specific targeting strategy employed. The characteristics of the nanoparticles also influence the cellular uptake, such as size, shape, surface, functionality/charge and aggregation state of nanoparticles (Alkilany & Murphy 2010, Dreaden et al. 2011, 2012).
Once inside the cells, nanoparticles are stored in endosomal/lysosomal vesicular structures. To release nanoparticles from these structures to the cytosol, their surface can be coated with membrane-disruptive peptides or can be modified with peptides which allow for direct transfer across the cell membrane (Sperling et al. 2008).

Regarding the cytotoxicity of gold nanoparticles, this field is somewhat controversial because toxicity may also depend on the cell lines used and the differences observed might perhaps be due to the different nature and properties of the various types of ligands. For example, cationic ligands can cause moderate toxicity due their ability to disrupt cell membranes. Despite the fact that the gold nanoparticle's core is considered inert and non-toxic, gold nanoparticles solutions ''as a whole'' can induce toxicity. This toxicity could rise from any part other than the core itself, such as capping agents used in gold nanoparticle synthesis and stabilization, leftover chemicals from the synthesis, ligands, recognition molecules, etc (Boisselier & Astruc 2009, Dreaden et al. 2012).

According to many reports, gold nanoparticles have been found to be nontoxic. Using a leukemia cell line, Connor et al reported that gold nanospheres of different sizes (4, 12, and 18 nm in diameter) and capping agents (citrate, cysteine, glucose, biotin, and cetyltrimethylammonium bromide) were found to be nontoxic based on MTT assays (Connor et al. 2005). Furthermore, Villiers et al. studied the toxicity of citrate-capped gold nanoparticles (spheres, 10 nm in diameter) on dendritic cells. They found that nanoparticles were not cytotoxic and did not change the phenotype of the studied cells (Villiers et al. 2010). In contrast

to these results, it was founded that gold nanoparticles less than 2 nm show evidence of chemical reactivity that does not occur at larger sizes (Turner et al. 2008).

The variability of results could be due to the different used toxicity assays, cell lines, and nanoparticles chemical/physical properties. Thus, a systematic toxicity study must be carried out for each specific case under precise conditions, before imaging, diagnosis and therapeutic applications of gold nanoparticles. Despite the importance of starting any toxicological screening using cell models, they do not provide results that can be extrapolated to conclude what the fate of these materials is *in vivo*. Thus, more *in vivo* studies are needed (Alkilany & Murphy 2010, Boisselier & Astruc 2009).

1.4 OBJECTIVES

The main goal of this project was to develop a gene delivery vector based on AuNPs to transfect a colorectal cancer cell line with EGFP expression vector and compare the efficiency with a commercial system (Lipofectamine). To achieve this goal various steps were needed:

1) Synthesis of citrate capped AuNP and functionalization with PEG;
2) AuNP@PEG functionalization with quaternary ammonium groups;
3) Binding of AuNP@PEG@R4N+ with EGFP expression vector via electrostatic interactions;
4) Characterization of AuNPs formulations;
5) Transfection studies with AuNP@PEG@R4N+@pEGFP in HCT-116 cancer cell line and evaluation of transfection efficiency by PCR and EGFP expression by fluorescence microscopy and fluorescence spectroscopy.

2. MATERIALS AND METHODS

2.1 NANOTECHNOLOGY

2.1.1 GOLD NANOPARTICLES SYNTHESIS

AuNPs were prepared by the reduction of tetrachloroaurate ($HAuCl_4$) with sodium citrate described by Turkevich (Turkevich et al. 1954) and improved by Lee and Miesel (Lee & Meisel 1982).

Prior to the synthesis of gold nanoparticles, all the glass material was treated with *aqua regia* (3:1 HCl:HNO_3) by immersion overnight. Then the material was washed with distilled water and mili-Q water (18.2 MΩ.cm^{-1} at 25ºC).

In a 500 mL round bottom flask, 250 ml of 1 mM HAuCl4 (Sigma, MW 393.83 Da) was heated and stirred. When in reflux, 25 ml of 38 mM sodium citrate (Sigma, MW 294.1 Da) was rapidly added and the mixture was kept in reflux for 20 minutes with continuous stirring. The colloidal solution was left to cool to room temperature while keeping the continuous stirring and was then transferred to a 500 mL Erlenmeyer flask and stored in the dark at room temperature.
The AuNPs were characterized by UV/Vis spectroscopy and their concentration was determined by the Lambert–Beer law assuming a calculated molar extinction coefficient for the plasmon resonance band maximum of $2.33x10^8$ $M^{-1}cm^{-1}$ (Baptista et al. 2005),Transmission Electron Microscopy and Dynamic Light Scattering.

2.1.2 AuNPs FUNCTIONALIZATION WITH PEG CHAINS

AuNPs were coated using a PEG functionalized with a thiol on one terminus and a carboxylated group on the other (SH-EG(8)-COOH, Iris.biotech, MW 458.57 Da). In order to achieve the concentration corresponding to 100% of PEG saturation of AuNP surface, a range of PEG concentrations were tested in a fixed amount of AuNPs.

The synthesis of PEGylated AuNPs was carried out by mixing 10 nM of AuNPs with PEG with a range of concentrations of 0 - 0.1 mg/ml PEG and 0.028% SDS (Sigma, MW 288.38 Da). Then the mixtures were incubated overnight on a GFL 3016 shaker at room temperature. To remove the non-ligated PEG chains, each mixture was centrifuged (Sigma 3-16K, UK) 3 times for 30 minutes at 14000 rpm, at 4ºC. The supernatants of the 3 washes were quantified by Ellman's Assay to determine the number of PEG chains per AuNP. In this assay, the thiol group present in supernatants reacts with DTNB (5,5´-dithio-bis-(2-nitrobenzoic acid), (Sigma, MW 396.35 Da) under alkaline conditions, giving a yellow solution which absorbance can be read at 412 nm.

The Ellman's assay was performed on a 96-well plate by mixing 200 µL of the supernatant of the 3 washes with 100 µL of phosphate buffer 0.5 M pH 7 – prepared by mixing 288.55 mM Na_2HPO_4 (Sigma) with 211.45 mM NaH_2PO_4 (Sigma) – and 7 µL of DTNB 2 mg/ml in phosphate buffer 0.5 M pH 7. After 10 minutes, the absorbance was measured at 412 nm. The number of bound PEG chains is given by the difference between the amount determined by Ellmans's assay and the initial amount incubated with the AuNPs.

The excess of PEG chains in the supernatants is quantified by interpolating a calibration curve set by replacing the supernatant with standard solutions of PEG (0.0002 – 0.5 mg/ml).

In this work, the PEG concentration used to cover the AuNPs surface was 0.035 mg/mL.

2.1.3 AuNPs FUNCTIONALIZATION WITH QUATERNARY AMMONIUM BY EDC/NHS COUPLING REACTION

AuNP@PEG was functionalized with quaternary ammonium ((2-aminoethyl)trimethylammonium chloride hydrochloride, Sigma, MW 175.1 Da) by EDC (1-Ethyl-3-(3-dimethylaminopropyl)-carbodiimide)/NHS (N-hydroxysulfoxuccinimide) coupling reaction.

For the functionalization, 21 nM AuNP@PEG was mixed with 1.25 mg/ml sulfo-NHS (Sigma, MW 217.13 Da), 10 mM MES pH 5.98 (Sigma, MW 195.24 Da) and 0.312 mg/ml EDC (Sigma, MW 191.7 Da) and incubated on a shaker for 30 min. Excess of reagents was removed by centrifugation for 30 minutes, at 14000 rpm and 4ºC. After this, quaternary ammonium was added to the mixture in a range of concentrations of 0 – 10 mg/ml. The mixture was incubated overnight at room temperature while stirring. The unbound quaternary ammonium was removed by centrifugation 3 times for 30 min, at 14000 rpm and 4º C.

In this work, the quaternary ammonium concentration used to functionalize AuNP@PEG was 7.5 mg/ml (Conde et al. 2012a).

2.1.4 FUNCTIONALIZATION OF AuNP@PEG@R_4N+ WITH pEGFP VECTOR

The complex formed between AuNP@PEG@R_4N^+ and the pEGFP vector (pVisionGFP-N vector 4.7 kb, Biovision – see section A1 in Appendix) is due to the positive charges of the quaternary ammonium groups and the negative charge of the pEGFP vector.

The complex was prepared by mixing AuNP@PEG@R_4N^+ at a final concentration of 10 nM with increasing amounts of the plasmid in sterile mili-Q water from 0.2 to 50 ng/µL (the pEGFP vector was always taken from a stock solution of 200 ng/µl in order to keep the same volume of

EGFP vector).The solutions were incubated at room temperature for 1h. After this time, the unbound vector was removed by centrifugation 1 time for 20 min, at 14000 rpm and 4º C.

The functionalization was assessed by UV/VIS spectroscopy, agarose gel electrophoresis and DLS measurements.

For the transfections studies, the concentration of EGFP expression vector used was 11 ng/μL.

2.1.5 DYNAMIC LIGHT SCATTERING MEASUREMENTS

To determine the hydrodynamic diameter of the naked and functionalized AuNPs, a set of DLS measurements was carried out. Thus, AuNPs were prepared in sterile mili-Q water at a final concentration of 2 nM and 1 ml of the sample was used for each measurement. Ten replicate measurements were obtained for each sample and each measurement lasts 30 seconds with a scattering angle of 90º at 25 ºC. DLS analysis was performed in Horiba SZ-100 Nanoparticle Analyzer in Departamento de Química (FCT/UNL).

2.1.6 TEM ANALYSIS

TEM analysis was performed with a HITACHI H-8100 microscope operated at 200 kV in Instituto de Ciência e Engenharia de Materiais e Superfícies (ICEMS/IST), Portugal (contracted service). The samples were prepared by depositing 10 μL of the as-prepared colloidal suspensions in carbon copper grids, washing twice with 10 μL of milli-Q water, and air dried.

Particle size and morphology were determined by analyzing the TEM pictures using the software image J.

2.2 MOLECULAR BIOLOGY

2.2.1 PREPARATION OF COMPETENT *E.coli* CELLS USING THE $CACL_2$ METHOD

E. *coli* cells (DH5α), stored at -80 ºC, were inoculated on a LB agar plate and incubated overnight at 37ºC. A single colony was inoculated in 3 ml of LB medium and incubated overnight at 37ºC, while shaking at 180 rpm. In the next morning, the culture was diluted (1:200) in the same medium and the growth was followed by measuring the optical density at 600 nm until it reached an OD_{600nm}=0.6. Cells were recovered by centrifugation at 7000 rpm for 5 min at 4ºC and then ressuspended in ½ of the initial volume in a 0.1 M $CaCl_2$ solution (Sigma, MW 110.95 Da) and stored on ice for 2 hours. Cells were recovered by centrifugation at 7000 rpm for 5 min at 4ºC and ressuspended in 1/15 of the initial volume in a 0.1M $CaCl_2$ and 15% (w/v) glycerol solution (Pronalab).

Competent cells were aliquoted in 100-150 µl fractions and stored at -80ºC.

2.2.2 *E.coli* TRANSFORMATION (based on the protocol by Ausubel et al., 1987)

Five microliters (2000 ng) of pEGFP vector were added to 50 µl of prepared *E.coli* competent cells and stored on ice for 50 min. The cells were then submitted to a heat shock at 42ºC for 90 seconds and rapidly transferred to ice during 5 min. Then 900 µl of LB medium were added and the cells were incubated for 1 hour at 37ºC, gently inverting the tubes every 10 min. Cells were recovered by centrifugation at 3000 rpm for 5 min and 850 µL of the supernatant were removed. Cells were ressuspended in the remaining volume (105 µL). After this, 100 µL of the transformed competent cells were cultured on LB agar plates with 30 µg/mL kanamycin (Life Technologies) and then incubated at 37ºC overnight. In the next day, an *E.coli* single colony of transformed competent cells was inoculated in 10 mL of LB medium supplemented with 30 µg/mL kanamycin and incubated overnight at 37ºC, 180 rpm.

Stock solutions of the transformed cells were prepared by adding 300 µL of glycerol to 700 µL of culture and stored at -80ºC.

2.2.3 *E. coli* PLASMID EXTRACTION

The plasmid extraction from E. *coli* was achieved using the alkaline lysis method.

In the day before extraction, 100 µL of an *E.coli* stock of transformed competent cells was inoculated in 10 mL of LB medium supplemented with 30 µg/mL kanamycin and incubated overnight at 37ºC, 180 rpm.

A volume of 1.5 mL of the culture was transferred to an eppendorf. Cells were pelleted by centrifugation at 12 000 rpm for 2 min in 1.5 mL eppendorfs. The supernatant was discarded and the pellet was ressuspended in 100 µL of ice-cold lysis I[1] solution and vortex to completely ressuspend cell pellet. After this, 200 µL of lysis II[1] solution were added and mixed by inversion. After 2 min on ice, 150 µL of lysis III[1] solution was added and vigorously mixed by vortex. After 5 min on ice, the lysate was centrifuged at 12 000 rpm for 5 min. 400 µL of the supernatant was transferred to a sterile eppendorf and 2 volumes of ice-cold 100% ethanol were added. The plasmid DNA was left to precipitate at -20ºC for 2h and then centrifuged at 12 000 rpm for 5 min. The supernatant was discarded and the pellet was washed with 1 ml of ice-cold 70% ethanol and left to air dry. The pellet was ressuspended in sterile mili-Q water. RNaseA (Fermentas) was added in a final concentration of 20 µg/mL and incubated for 2 hours at 37ºC. After this time, one extraction with 1 volume of phenol was performed, followed by one extraction with chloroform/isoamyl alcohol (24:1). Two volumes of absolute ethanol were added

to aqueous phase and the plasmid DNA was left to precipitate at- 20ºC for 2h like described above. Plasmid DNA was ressuspended in sterile mili-Q water and stored at 4 ºC.

The plasmid extracted was quantified using the UV-Vis Spectrophotometer Nanodrop ND-1000 (Nanodrop Technologies, USA).

[1] Lysis solutions preparation is showing in appendix in section A2

2.3 PCR FOR THE AMPLIFICATION OF THE GENE ENCODING EGFP AND FTO GENE

The primers used for PCR to amplify the gene encoding the enhanced green fluorescence protein are shown in Table 2.1, as well as the expected product length determined using the tool "*Primer-Blast*" (http://www.ncbi.nlm.nih.gov/tools/primer-blast/). The complete reaction program is described in Table 2.2.

The PCR was performed in a MyCycler Thermal Cycler (BioRad, Califórnia, EUA) and the reaction mixture was prepared in a 200 μL microtube by adding 1x Taq Buffer (Fermentas, Canada), 1 mM dNTPs (Bioline, United Kingdom), 0.5 μM EFGP primer forward (StabVida, Portugal), 0.5 μM EFGP primer reverse (StabVida, Portugal), 2 U DreamTaq DNA polymerase (Fermentas, Canada), and sterile mili-Q water to bring the volume to 20 μL. The amount of template used was 20 ng.

Table 2.1 – Primers sequence used in PCR reaction to EGFP and FTO gene.

Primers	Sequence (5'- 3')	Product length (bp)
EGFP Forward	agcttcgaattctgcagt cg	806
EGFP Reverse	ggctgattatgatctagagtc	
FTO Forward	ttc aaa act ggc tct tga agt	225
FTO Reverse	cag tca gaa atg gag tgg gag	

Table 2.2 – Reaction Program to amplify the gene encoding EGFP.

	Temperature (ºC)	Time	Cycles
Initial Denaturation	95	1 min	1
Denaturation	95	30s	30
Annealing	57.5	30s	
Extension	72	1 min	
Final Extension	72	10 min	1

FTO gene (housekeeping gene) was used as internal control of transfection studies. PCR for FTO gene was performed by adding in a 200 μL microtube 1.5 x Hot Taq Buffer (StabVida, Portugal), 2.5 mM MgCl2 (StabVida, Portugal), 0.2 mM dNTPs (Fermentas, Canada), 0.4 μM FTO primer forward (StabVida, Portugal), 0.4 μM FTO primer reverse (StabVida, Portugal), 2 U Hot Taq DNA polymerase (StabVida, Portugal) and sterile mili Q water to bring the volume to 25 μL. The amount of template used was 20 ng.

Table 2.3 – Reaction Program to amplify FTO gene.

	Temperature (ºC)	**Time**	**Cycles**
Initial Denaturation	95 ºC	15 min	1
Denaturation	94 ºC	1 min	35
Annealing	60 ºC	30 s	
Extension	70 ºC	30 s	
Final Extension	70 ºC	6 min	1

PCR products were analyzed by 1% agarose gel electrophoresis (1x TAE, 60 V, and 1h 30).

2.4 CELL CULTURE MANIPULATION

HCT-116 cells (from colorectal carcinoma) were grown in Dulbecco's modified Eagle's medium with Glutamax (DMEM, Invitrogen) with 10% heat inactivated fetal bovine serum (FBS, Invitrogen), 100 U/mL penicillin and 100 µg/mL streptomycin (Invitrogen). Cells were maintained in a CO_2 incubator with 5% (v/v) CO_2, at 37ºC in 99 % humidified atmosphere in 75 cm^2 culture flask (VWR).

Cell cultures were transferred to a new cell culture flask upon reaching a confluence of about 80%, which was verified by inverted optical microscopy (Nikon TMS). To this end, all medium was aspirated, cells were washed once with 1x PBS pH 7.4, 2 ml trypsin 1x (Invitrogen) was added and the flask was placed in the CO_2 incubator for 5 min. Once all cells were detached from the flask, 8 mL of fresh serum-containing medium was added to neutralize the trypsin action. Fifteen mL of growth medium was placed in a new 75 cm^2 culture flask and 500 μL of cells were added to the flask. Cells were grown for 18 - 24h in a CO_2 incubator prior to any experiment was performed.

2.4.1 DETERMINATION OF CELL CONCENTRATION

For the transfection studies, a certain number of cells are needed. To perform the cell count, 20 μL of cells were mixed with 80 μL of Trypan Blue 0.4% (m/v) (Sigma). Ten μL of this mixture was then added to a Neubauer chamber (Hirschmann, Germany) and the viable cells were

counted by visualization on an inverted microscope. Trypan blue is a dye that is capable of trespassing the plasma membrane of non-viable cells, since these cells have a more permeable cell membrane. Thus, cells that are viable do not have any coloration whereas non-viable cells are blue. The number of cells per mL is given by the equation (1):

$$\frac{No.\ of\ viable\ cells}{mL} = \frac{\Sigma no.of\ viable\ cells\ of quadrants\ 1\ to\ 4}{4} x10^4 \text{ x dilution factor} \qquad (1)$$

2.5 TRANSFECTIONS STUDIES

2.5.1 EGFP VECTOR TRANSFECTION

In order to study the transfection efficiency of the gold nanoparticles conjugates, transfection experiments were performed in HCT-116 cells.

HCT-116 cells were seeded at a density of 1 x 10^5cells/well in 24-well plate in 500 μL of DMEM, maintained at 37º C in 5% CO_2 and grown for 24 h prior to transfection. On the day of transfection, cells were approximately 80% of confluence. Thus, the medium was removed, cells were washed 1 time with 1x PBS pH 7.4 and 400 μL of DMEM was added to each well. The complex AuNP@PEG@R_4N^+@pEGFP functionalized with 11 ng/μL was freshly prepared and 100 μL of the complex were added to each well, containing 400 μL of DMEM, in order to get a final amount of pEGFP vector of 1 μg per well.

As a positive control Lipofectamine 2000 (Invitrogen) was used as the transfection reagent, according to manufacturer's protocol. The lipoplex is formed according to a ratio DNA (μg):Lipofectamine 2000 (μl) of 1:2.

For 24-well plate, 1 μg (5 μL of a stock solution of 200 ng/μL) of EGFP vector was diluted in 45 μL of Opti-MEM reduced serum medium and 2 μL of Lipofectamine 2000 was diluted in 48 μL of the same medium. After 5 min of incubation, EGFP vector solution was added to Lipofectamine 2000 solution, mixed gently, and incubated for another 20 min at room temperature to allow lipoplex formation. After this time, 400 μL of DMEM antibiotic free was added to the complex and then added to the cell-containing wells.

The transfection efficiency was evaluated by fluorescence spectroscopy, fluorescence microscopy and PCR at different incubation times from 3 to 48h.

2.5.2 FLUORESCENCE MICROSCOPY

HCT-116 cells were seeded at a concentration of 1 x 10^5 cells/well in 24-well plate over glass coverslips in 500 μL of DMEM (Invitrogen) with 10% heat-inactivated fetal bovine serum (Invitrogen) and maintained at 37 º C in 5% CO_2 (grown for 24 h prior to transfection). The transfection was performed as described in section 2.5.1. EGFP expression was assessed at different incubation times from 3 to 24h.

After each incubation time, cells were washed 1 time with 1x PBS pH 7.4 and fixed with 4% paraformaldehyde in PBS for 15 min. The glass coverslips was washed 3 times with 1x PBS pH 7.4 and mounted in 10 μL ProLong Gold Antifade Reagent with DAPI (Invitrogen) to allow for nuclear staining. The glass slides were observed in an Axioplan 2 microscope (Zeiss, Germany).

2.5.3 EGFP EXPRESSION EVALUATION BY FLUORESCENCE SPECTROSCOPY

EGFP expression was evaluated by fluorescence spectroscopy at different incubation times from 3 to 48h. Thus, all medium was removed; cells were washed with 1x PBS (to remove the cell culture medium) and 100 μL of sterile mili-Q water was added to each well. The plate was placed on a shaker for 30 min in order to lyse the cells by osmotic shock. After vigorous shaking, the lysate was transferred to 1.5 mL tubes and briefly sonicated and centrifuged at 13 000 g for 25 min at 4ºC.

EGFP fluorescence was determined by placing 70 μL of the lysate in a quartz cuvette, and using a Varian Cary Eclipse spectrofluorimeter, in a range 490-650 nm, after excitation at 480 nm.

2.5.4 EVALUATION OF AuNP UPTAKE BY CELLS

In order to confirm the uptake of the nanoconjugate AuNP@PEG@R_4N^+@pEGFP by cells and confirm the presence of the plasmid inside the cells, a PCR was performed to amplify the gene encoding EGFP.

This assay was performed incubating the nanoconjugate and Lipofectamine 2000, as described in section 2.5.1, at different time points of 3h, 6h, 12h and 24h. After incubation time, the medium was removed and the wells were washed three times with 1x PBS pH 7. Cells were detached adding 100 μL trypsin 1x and the plate was placed in CO_2 incubator for 5 min. Once all of the cells have detached, 400 μL of DMED were added to neutralize the trypsin action and the total 500 μL were transferred to an eppendorf tube for DNA extraction.

Total DNA was extracted from cells transfected with Lipofectamine 2000 (positive control) and nanoconjugates, and non-transfected cells (negative control) using *QIAamp DNA Mini Kit* (Qiagen) and quantified using the UV-vis Spectrophotometer Nanodrop ND-1000. The DNA extracted was used to perform the PCR using the primers presented in Table 2.1 and the reaction program described in Table 2.2, presented in section 2.3. As internal control, FTO gene was used and the primers, as well as the reaction program, are described in Tables 2.1 and 2.3 in section 2.3.

2.6 MTS ASSAY

Standard MTS (3-(4,5-dimethylthiazol-2-yl)-5-(3-carboxymethoxyphenyl)-2-(4-sulfophenyl)-2H-tetrazolium) assay was performed to determine the cytotoxicity of the functionalized AuNP complexes compared with the Lipofectamine 2000. When MTS is exposed to PMS, it is converted into formazan by viable cells which are brown. Thus, this colorimetric method is often used to determine the number of viable cells

HCT-116 cells were transfected in 96-well plates as described in section 2.4.1 but using a cell density of 1 x 10^4cells/well and incubated for 48h. The viability was assessed using Kit CellTiter 96 AQueous Non-Radioactive Cell Proliferation Assay (Promega, Madison, EUA) according to the manufacturer's protocol. After the incubation time, the culture medium was removed from each well and replaced by 100 μL of MTS solution in a ratio of 100:20:1 of DMEM, MTS and PMS, respectively. The plate was incubated for 30 min in a CO_2 incubator with 5 % (v/v) CO_2, at 37ºC. Then the absorbance at 490 nm was measured in a Microplate reader Infinite M200 (Tecan, Smitzerland) and the cell viability was given by the equation (2):

$$\text{Cell viability } (\%) = \frac{Abs\ 490\ nm\ (sample)}{Abs\ 490\ nm\ (control)} \text{ x } 100 \qquad (2)$$

3. RESULTS AND DISCUSSION

3.1 GOLD NANOPARTICLES SYNTHESIS AND CHARACTERIZATION

The synthesis of gold nanoparticles was achieve by reduction of sodium tetrachloroaurate (III) hydrate with sodium citrate dehydrate, yielding AuNPs with an average diameter of 14 nm. AuNPs characterization by UV-vis spectroscopy revealed a single absorbance band in 521 nm due to the localized surface plasmon resonance (LSPR). The spectrum indicates relatively monodisperse spherical particles due the symmetric absorption peak at 521 nm (see Figure 3.1b). The concentration of AuNPs was determined via the Lambert-Beer equation, assuming an extinction coefficient of 2.33 x 10^8 M^{-1} cm^{-1} for the plasmon resonance band (Baptista et al. 2005), resulting in a concentration of about 14 nM.

TEM analysis provides direct visualization of morphology and size distribution of synthesized AuNPs. TEM image shown in Figure 3.1a confirms the data of the UV-vis. The diameter determined from TEM image using the software Image J was 14.28 nm (± 0.2), which was in agreement with the hydrodynamic diameter determined by DLS, 14.14 nm (± 0.4).

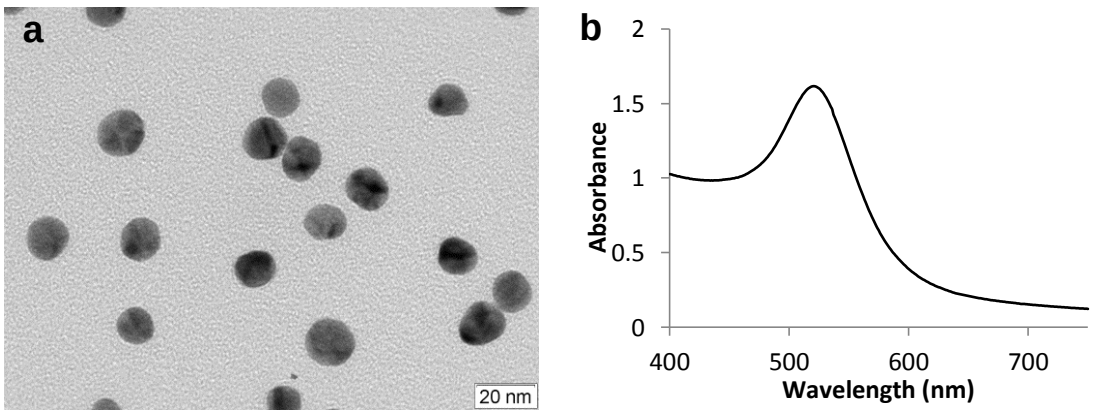

Figure 3.1 - Characterization of the synthesized AuNPs: (a) Transmission electron microscopy (TEM) showing monodispersed spherical AuNPs (scale bar 20 nm); (b) UV-vis spectrum of the synthesized gold nanoparticles revealing a SPR band at 521 nm.

3.2 GOLD NANOPARTICLES FUNCIONALIZATION

3.2.1 POLY (ETHYLENE GLYCOL) (PEG)

To increase the stability, biocompatibility and allow chemical functionality with quaternary ammonium groups, citrate capped AuNPs were functionalized with a thiolated poly (ethylene glycol) (PEG) (HS-PEG(8)-COOH). This polymer is a water-absorbing molecule that has the ability to attract water molecules, creating a shield around the AuNPs, which allows them to

travel through the body's blood vessels and which increases the stability and biocompatibility of the nanocarrier.

The PEGylation of the AuNPs occurs through the complete exchange of the citrate molecules surrounding the AuNPs surface with PEG chains, creating an Au-S quasi-covalent bond. The carboxylated group provides the anchoring moieties for the covalent binding of amine-containing molecules through carbodiimide chemistry.

In order to produce AuNPs capped with a 100% saturation layer of PEG, various concentrations of PEG were added to the synthesized AuNPs from 0 – 0.1 mg/ml. The excess of PEG was removed by centrifugation and the supernatants resulting from the three washes were quantified by the Ellmans's assay, by interpolating the calibration curve shown in Figure 3.2a. The number of bound chains to the AuNPs surface was given by the difference between the amount determined by this assay and the initial amount of chains in the incubation mixture. It was determined that the maximum coverage per AuNP was 0.035 mg/ml, because it was the concentration where PEG molecules were detected in the supernatant. Thus, gold nanoparticles were functionalized with 0.035 mg/mL of SH-PEG(8)-COOH, corresponding to 100% of PEG saturation of AuNP surface (4300 $\pm$ 114 chains/AuNP).

Figure 3.2 b shows the excess of PEG in the first supernatant as a function of the initial concentration in an incubation mixture. As the initial PEG concentration increases, the excess of free PEG increases. There was a point at which the AuNP becomes saturated with a PEG layer and was not able to uptake more PEG chains, that is 0.035 mg/ml.

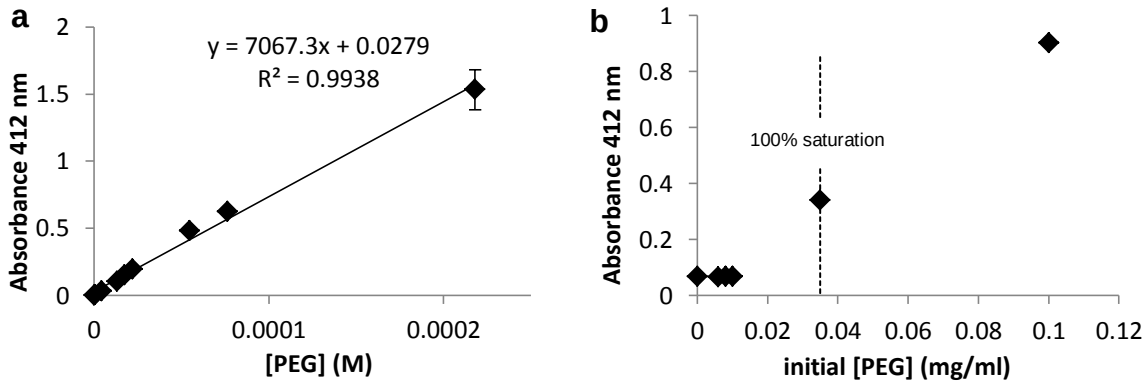

Figure 3.2 **–** (a) Standard calibration curve for PEG chains, whose concentration can be calculated via the following equation Abs_{412nm} = 7067.3 x [PEG] (M) + 0.0279. (b) Variation of the excess of PEG thiolated chains as a function of the initial concentration in the incubation with 10 nM AuNPs. The vertical line indicates the 100% saturation, i.e. the PEG concentration above which no more PEG can be bound to the AuNP surface.

Once determined the ideal concentration to fully cover AuNP surface as well PEG chain/AuNP, UV-vis and DLS analysis were performed to characterize the functionalized AuNPs. UV-vis

spectrum exhibited a shift on the SPR band from 521 to 524 nm, a 3 nm shift for PEG binding, meaning an increase in the diameter (see Figure 3.3). To confirm the functionalization, the AuNPs were analyzed by DLS, which reveals an increase in hydrodynamic diameter from 14.14 nm to 35.2 nm (± 1.2). The length of a PEG chain is 3.25 nm (www.iris-biotech.de), so it would be expected an increase of the diameter of 6.5 nm, instead of 21.06 nm. The difference between expected values and experimental values can be explained by the formation of multiple layers of PEG on the AuNPs surface. Furthermore, PEG is a flexible polymer that can change the Brownian motion of the AuNPs, thus introducing a frictional drag and reducing the diffusion of the AuNP. This results in an increase of the hydrodynamic diameter of the AuNP.

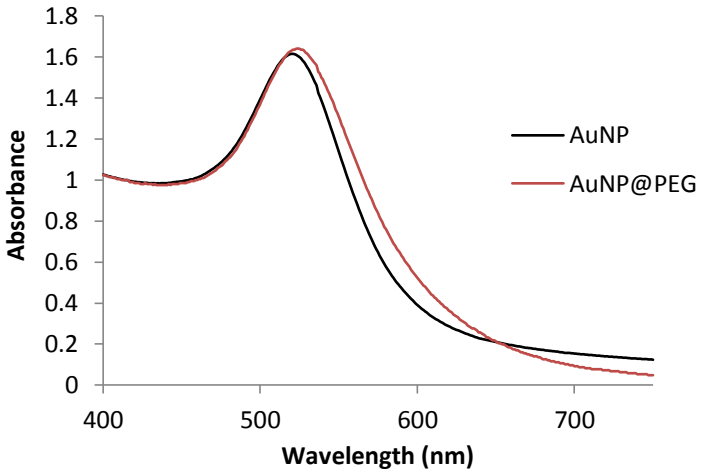

Figure 3.3 – UV-vis spectra of synthesized AuNPs and coated with PEG chains, revealing a shift from 521 to 524 nm, a 3 nm shift of the SPR band for PEG binding.

3.2.2 QUATERNARY AMMONIUM

Gold nanoparticles functionalization with (2-Aminoethyl)trimethylammonium chloride hydrochloride was carried out via an EDC/NHS reaction, which created a bond between the carboxylated PEG spacer and the amine group of (2-aminoethyl)trimethylammonium hydrochloride.

It has been showed that quaternary ammonium groups are capable to bind plasmid DNA through electrostatic interactions and that it can protect DNA from enzymatic digestion (Han et al. 2006, McIntosh et al. 2001). These cationic groups have also been described as having a possible proton sponge effect played by the carboxylic group and quaternary ammonium groups, which could be responsible for endosome rupture and release of the trapped materials into the cytoplasm (Yezhelyev et al. 2008).

To determine the optimal of ammonium groups to get full coverage of the gold nanoparticle surface, a range of concentrations from 0 – 10 mg/ml (2-Aminoethyl)trimethylammonium chloride hydrochloride were mixed with 21 nM of AuNPs. Since it was not possible to quantify the amine groups in the supernatants, the functionalization was evaluated by UV-vis

spectroscopy (see Figure 3.4) and through the work developed by Conde et al., where an ionic approach was employed to bind siRNA to 14 nm AuNP coated with PEG and the same quaternary ammonium compound used in this work (Conde et al. 2012a).

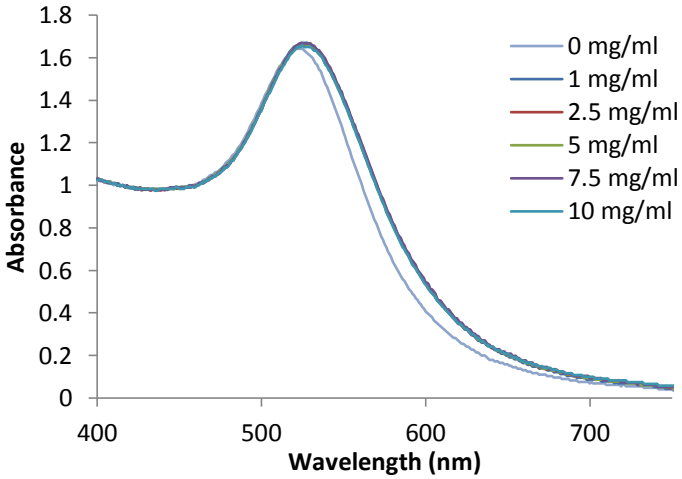

Figure 3.4 – UV-vis spectra of AuNP@PEG coated with increase amount of quaternary ammonium. When the R_4N^+ group is not added, SPR absorption band is located at 523 nm, while in the presence of quaternary ammonium a shift to 526 nm is observed.

The functionalization was evaluated through UV-vis spectroscopy, since the SPR band is dependent on the size, shape, aggregation state and medium polarity. As shown in Figure 3.4, a shift in the surface plasmon resonance band from 523 to 526 nm was observed in samples where increasing amounts of quaternary ammonium were added (0 – 10 mg/ml). This shift to 526 nm may be associated to an increase in the diameter and a change in the chemical environment surrounding the AuNP@PEG surface. Since the shift was the same for any concentration, it appears that the environment surrounding the AuNP@PEG surface was the same, and above 1 mg/ml no more quaternary ammonium can be bound to the AuNP@PEG surface.

Since these results were not conclusive, the quaternary ammonium concentration used to cover the AuNP@PEG surface was 7.5 mg/ml and the nanoconjugate was characterized by UV-vis spectroscopy and DLS. This value was extrapolated from the work developed by Conde et al. in which a similar formulation was developed (Conde et al. 2012a).

As shown in Figure 3.5, the double functionalization of the AuNPs (PEG plus quaternary ammonium molecules) results in a shift of the SPR band towards larger wavelengths, which may be associated to changes in the dielectric environment surrounding AuNPs. When functionalized with 7.5 mg/ml of quaternary ammonium, the spectrum of AuNP@PEG exhibits a 2 nm shift from 524 to 526 nm, meaning an increase in the diameter. DLS analysis reveals an increase in hydrodynamic diameter from 35.2 to 43.9 nm (±1). A large increase on the

hydrodynamic diameter was not expected since quaternary ammonium groups show a small molecular footprint (Yezhelyev et al. 2008).

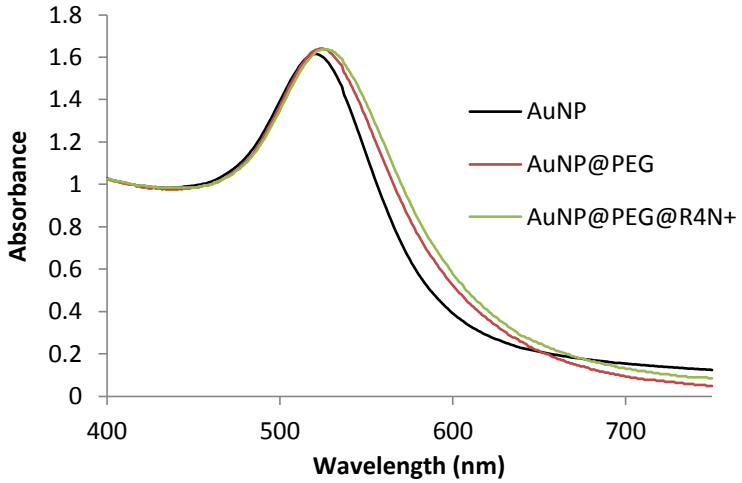

Figure 3.5 – UV-vis spectra of synthesized AuNPs, AuNP@PEG and AuNP@PEG coated with 7.5 mg/ml of quaternary ammonium, revealing a shift from 524 (AuNP@PEG) to 526 nm, a 2 nm shift of the SPR band for quaternary ammonium binding.

3.2.3 EGFP PLASMID BINDING TO AuNP@PEG@R_4N+

Due the strong negative charge of nucleic acids, the nanoconjugate AuNP@PEG@R_4N^+ has the ability to bind plasmid DNA thought electrostatic interaction, since the surface of the AuNP-based formulation is positively charged. An analogous complex was described by Sandhu et al. who created a delivery vehicle to bind plasmid DNA using quaternary ammonium–functionalized AuNPs (Sandhu et al. 2002) with a gold core of 2 nm and a total diameter of 6 nm. In these AuNP@DNA complexes, the DNA is bent around the AuNPs into a “spaghetti and meatballs” motif, protecting the DNA from degradation.

To study the interaction between nanoconjugate and plasmid DNA, increase amounts of pDNA were added to a fixed concentration of AuNP@PEG@R_4N^+ (10 nM). After 1 hour of incubation at room temperature, the samples were centrifuge one time for 25 min at 14000 rpm at 4ºC to eliminate the unbound pDNA. This binding was studied by UV-vis spectroscopy using the surface plasmon resonance of the gold nanoparticles as indicator of functionalization and the absorbance at 260 nm. Thus, spectra of these samples were taken in a range from 200 – 750 nm.

The absorbance spectra obtained from the assay described above are shown on Figure 3.6. Regarding to the SPR band, it was observed that the greater the concentration of pDNA added, the greater the red-shift (see Table 3.1), which may be indicative that there was always plasmid bound to AuNPs.

Table 3.1 – SPR band of the AuNP@PEG@R_4N^+@pEGFP, which increases with increasing concentration of pEGFP.

[pEGFP]	0.2 ng/μL	0.5 ng/μL	1 ng/μL	2 ng/μL	11 ng/μL	50 ng/μL
SPR (nm)	526	528	529	531	533	~ 650

Regarding the absorbance around 260 nm, corresponding to the absorption maximum of nucleic acids, an opposite behaviour was observed and there was a trend in which the greater the concentration of pDNA, the lower the absorbance at 260 nm. This may be due to conformational changes to the pDNA, such as increased condensation, forming of aggregates and/or strand stacking, leading to a hypochromic effect (Ozluer & Kara 2014).

Concerning the sample related to 50 ng/μL pDNA, it was observed a change in the color or the AuNPs from red to purple-blue. This color change caused a shift to a wavelength of 650 nm, which is indicative of AuNPs aggregation.

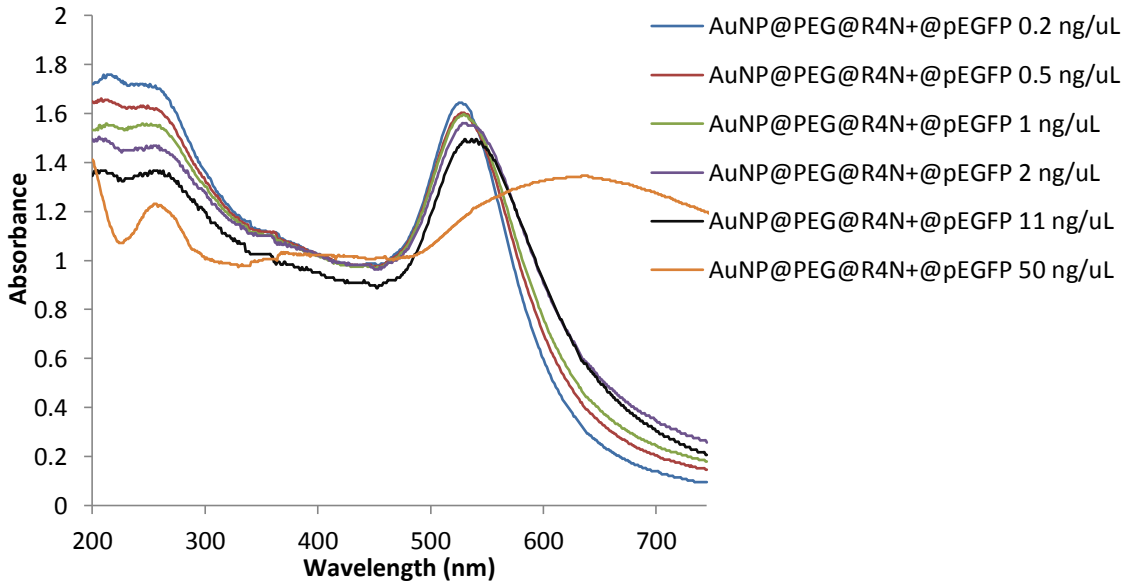

Figure 3.6 – UV-vis spectra of AuNP@PEG@R_4N^+@pEGFP were taken 1h after addition of the plasmid and centrifuge one time. A shift on SPR band to larger wavelengths was observed as the concentration of plasmid increased.

Figure 3.7, reveals the importance of including R_4N^+ groups to ensure electrostatic interactions between the positively charged AuNPs and the negatively charged pDNA. There was no shift observed in surface plasmon resonance band when AuNP@PEG was incubated with pEGFP, remaining the peak at 523 nm. So, it was possible to conclude that the binding of plasmid to gold nanoparticles surface was exclusive due to quaternary ammonium groups.

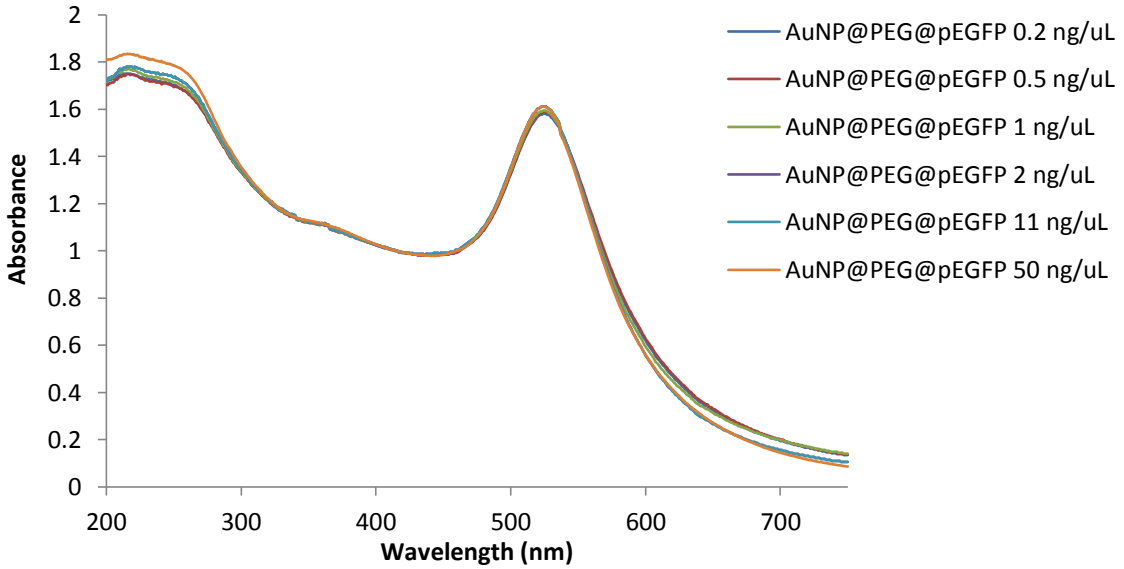

Figure 3.7 – UV-Vis spectra of AuNP@PEG@DNA were taken 1h after addition of the pDNA and centrifuge one time. No binding of the pDNA was observed, once no shift on the SPR band was observed and the absorbance at 260 nm suffered no change.

The functionalization was also assessed by agarose gel electrophoresis and the hydrodynamic diameter of the complex was determined by DLS analysis.

Gel electrophoresis was carried out initially to test the association of AuNPs with pEGFP. Thus, the samples corresponding to the spectra shown in Figures 3.6 and 3.7, as well as their supernatants were submitted to an electrophoretic analysis in agarose gel, as shown in Figure 3.8.

It is possible to observe a complete inhibition of electrophoretic mobility of the plasmid when pDNA was complexed to the AuNP@PEG@R_4N^+ in a range of concentrations of 0.2 – 11 ng/μL; no electrophoretic mobility of pDNA for samples and their respective supernatants in lane 2 – 6 and lane 8 – 12, respectively. This suggests that the complex was completely neutralized and the entire plasmid was bound or the complex was too large to migrate into the gel. An electrophoretic mobility of pDNA toward the positive electrode was observed in the supernatant of the sample where AuNP@PEG@R_4N^+ was incubated with 50 ng/μL of pDNA, (lane 13), suggesting that an excess of pDNA was present and did not bind to the AuNPs.

To confirm that pDNA was incapable to bind to AuNPs in the lack of quaternary ammonium groups, these samples and theirs supernatant were also submitted to an electrophoretic analysis in agarose gel (see Figure 3.8). In the case of the samples (lane 14 – 19), plasmid was not observed indicating that this did not bind to the AuNP@PEG. As can be seen in lane 22 – 25, the plasmid did not bind to the AuNPs and consequently came out in supernatants. At lower concentrations (0.2 and 0.5 ng/μL, lane 20 and 21, respectively), electrophoretic mobility of the

pDNA is almost not visible probably because these concentrations are very close to the detection limit of the technique (0.1 ng DNA to GelRed stain (www.biotium.com)). Once again, it can be concluded that the binding of plasmid to AuNPs is due to the presence of quaternary ammonium groups.

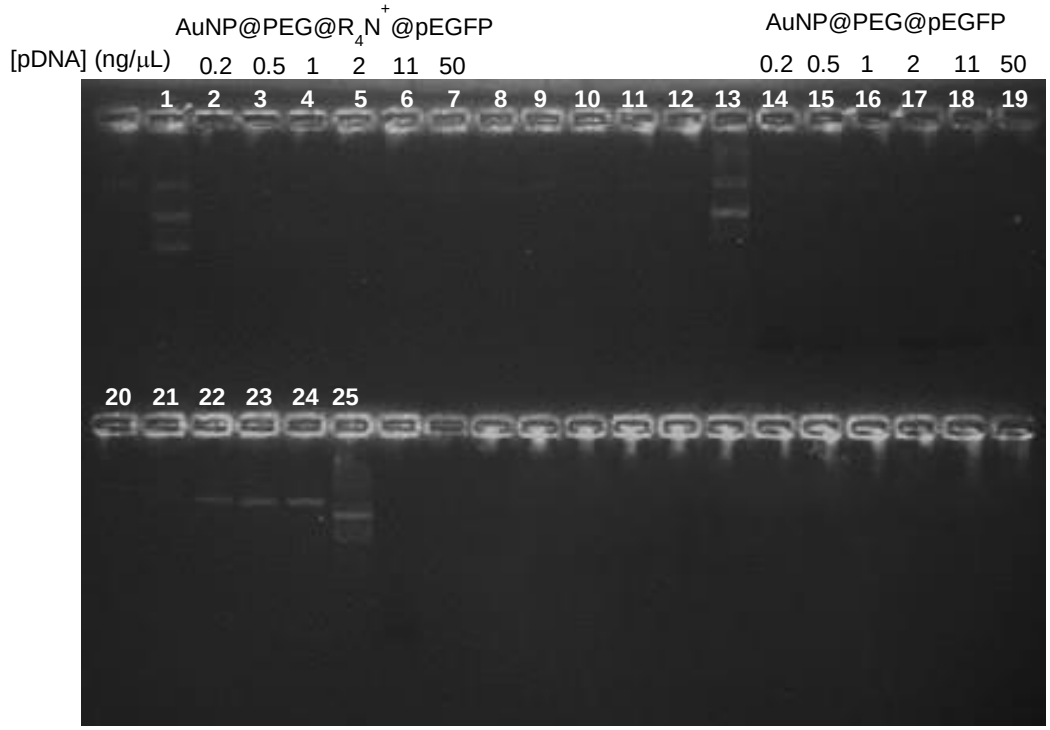

Figure 3.8 – Agarose gel electrophoresis (1%, TAE 1x, 80 V for 60 min) of AuNP@PEG@R_4N^+@pEGFPcomplexes prepared at the concentrations of pEGFP (0.2 – 50 ng/μl) given on top with a fixed amount of AuNPs (10 nM): lane 1 – plasmid DNA only; lane 2 - 7 – AuNP@PEG@R_4N^+@pEGFP 0.2 – 50 ng/μl; lane 8 - 13 – supernatants from the samples AuNP@PEG@R_4N^+@pEGFP 0.2 – 50 ng/μl; lane 14 - 19 – AuNP@PEG@ pEGFP 0.2 – 50 ng/μl; lane 20 - 25 – supernatants from the samples AuNP@PEG@pEGFP 0.2 – 50 ng/μl.

The concentration of the plasmid bound on the AuNPs surface intended to transfect cells (1 μg) was 11 ng/μL. This amount was selected for transfection because it was the same amount transfected with Lipofectamine 2000 and would allow for direct comparison of efficiency. DLS analysis was performed with the AuNP complex functionalized with 11 ng/μL in order to obtain the hydrodynamic diameter.

DLS analysis reveals a hydrodynamic diameter of 113.5 nm (± 0.8), an increase of 69.6 nm in relation to AuNP@PEG@R_4N^+. The diameter of the plasmid is dependent of the size, conformation, charge, temperature and solvent. Thus, it is difficult to predict the increase in the diameter of AuNPs. Furthermore, plasmids change conformation to bind to the AuNPs surface, which adds to size variations (Sandhu et al. 2002).

Despite the size of the nanoconjugates, internalization by cells was still expected as reported by Gosh et al. using amino acid-coated nanoparticles with a diameter around 100 nm, which were efficiently internalized with β-gal plasmid in mammalian cells (Ghosh et al. 2008).

Regarding the SPR band of the AuNP@PEG@R_4N^+@pEGFP functionalized with 11 ng/μL of pEGFP, a 7 nm shift occurred from 526 to 533 nm, when the plasmid was bound to AuNPs surface (see Figure 3.9). This shift is associated to the increases of the AuNPs diameter and by charge alterations on the surface of the AuNPs. While the functionalization with quaternary ammonium groups turn the surface more positive, binding of the plasmid makes them slightly less positive. Plasmid binding led to a shift in SPR band once this is dependent of factors such as size, shape, and charge surface.

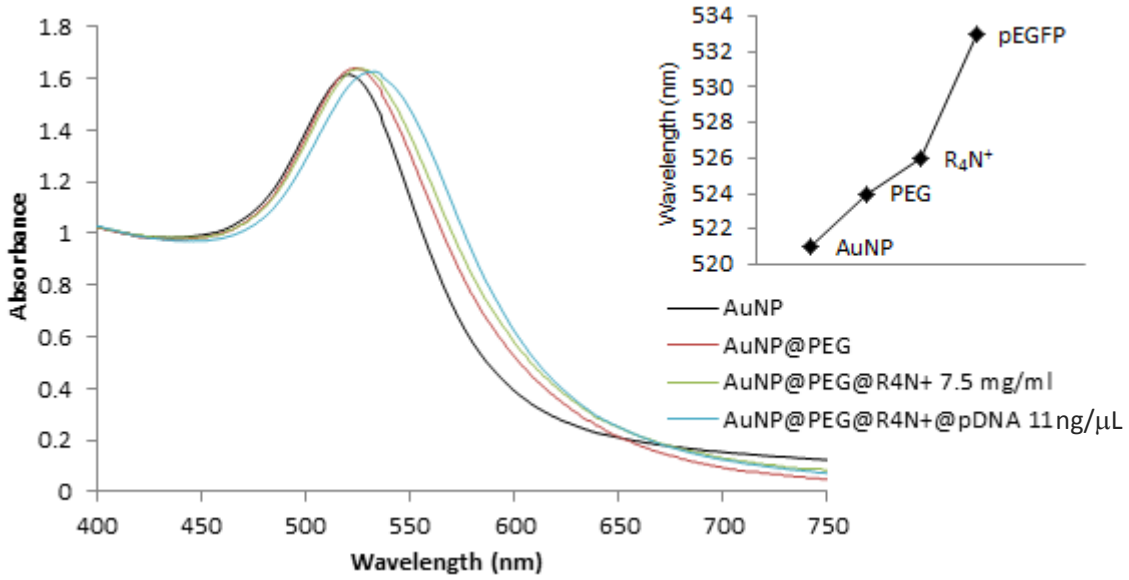

Figure 3.9 – UV-vis spectra of synthesized AuNPs and functionalized with PEG, quaternary ammoniums and pEGFP. The SPR band exhibited a shift to major wavelengths while the different groups bound to AuNPs surface.

Once no plasmid was detected in the supernatant when plasmid was attached on AuNPs, it was considered that all plasmid was bound on AuNPs surface. Thus, for the transfection studies, no more centrifugations were done so as to avoid unnecessary precipitation of some AuNPs in the walls of the tubes, which alters the concentration of the AuNPs and consequently the amount required for transfection (the spectrum of the complex shown in Figure 3.9 was taken without further centrifugation).

With the results presented until now, it was possible to conclude that the AuNP-based formulation developed would be capable to be used as a vehicle to transport the plasmid inside the cells in order to express EGFP protein.

3.3 TRANSFECTION STUDIES

To assess the potential of the AuNP@PEG@R_4N^+@pEGFP as gene delivery, colorectal cancer (HCT-116) cells were transfected with an EGFP expression vector complexed on the AuNP-based formulation. These cells were chosen due to the relevance of colorectal carcinoma (see section 1.1) and also due to the extensive expertise within the Nanomedicine@FCT group in transfecting EGFP plasmid using Lipofectamine 2000 (Conde et al. 2014b). The ability of the nanoconjugates to deliver the EGFP vector was compared to the standard pDNA transfection using Lipofectamine 2000.

To make this comparison possible, the amount of EGFP expression vector used in transfection assays was 1 μg in both Lipofectamine 2000 (according to manufacturer's protocol) and the nanoconjugate. In the case of the nanoconjugate used in transfection assay, this was functionalized using a concentration of 11 ng/μl because this was the concentration in which the amount desired to transfect (1 μg) was complexed to the AuNPs.

Transfection efficiency is the most important factor to assess the quality of gene delivery vectors and measuring the intracellular expression of EGFP is an excellent way to investigate the quality of the delivery vector developed. Thus, EGFP expression was assessed by fluorescence microscopy and fluorescence spectroscopy.

3.3.1 EGFP EXPRESSION EVALUATION BY FLUORESCENCE SPECTROSCOPY AND FLUORESCENCE MICROSCOPY

Previous studies, reported by Vaughan & Dean, where a GFP expressing plasmid was microinjected into the cytoplasm of cultured cells, showed a significant level of expression after 4 hours (Vaughan & Dean 2006). Thus, EGFP expression was evaluated at different incubations times from 3 – 48 h, in order to follow the increase of the expression.

Images of fluorescence microscopy were acquired using two different filters. To visualize DAPI stain, which allows imaging of the cell nucleus (DAPI emission 461 nm), the blue filter was used (range 430 – 465 nm) and to assess EGFP expression, a green filter was used (range 500 – 550 nm). Figure 3.10a shows these images of the non transfected cells (control) and cells transfected with Lipofectamine 2000 and AuNP@PEG@R_4N^+@pEGFP that were acquired after 3h and 6h incubation. The relative EGFP expression 3h and 6h post transfection is also represented in Figure 3.10b and was acquired measuring the fluorescence intensity of cell lysates, after excitation at 480 nm and emission at 510 nm.

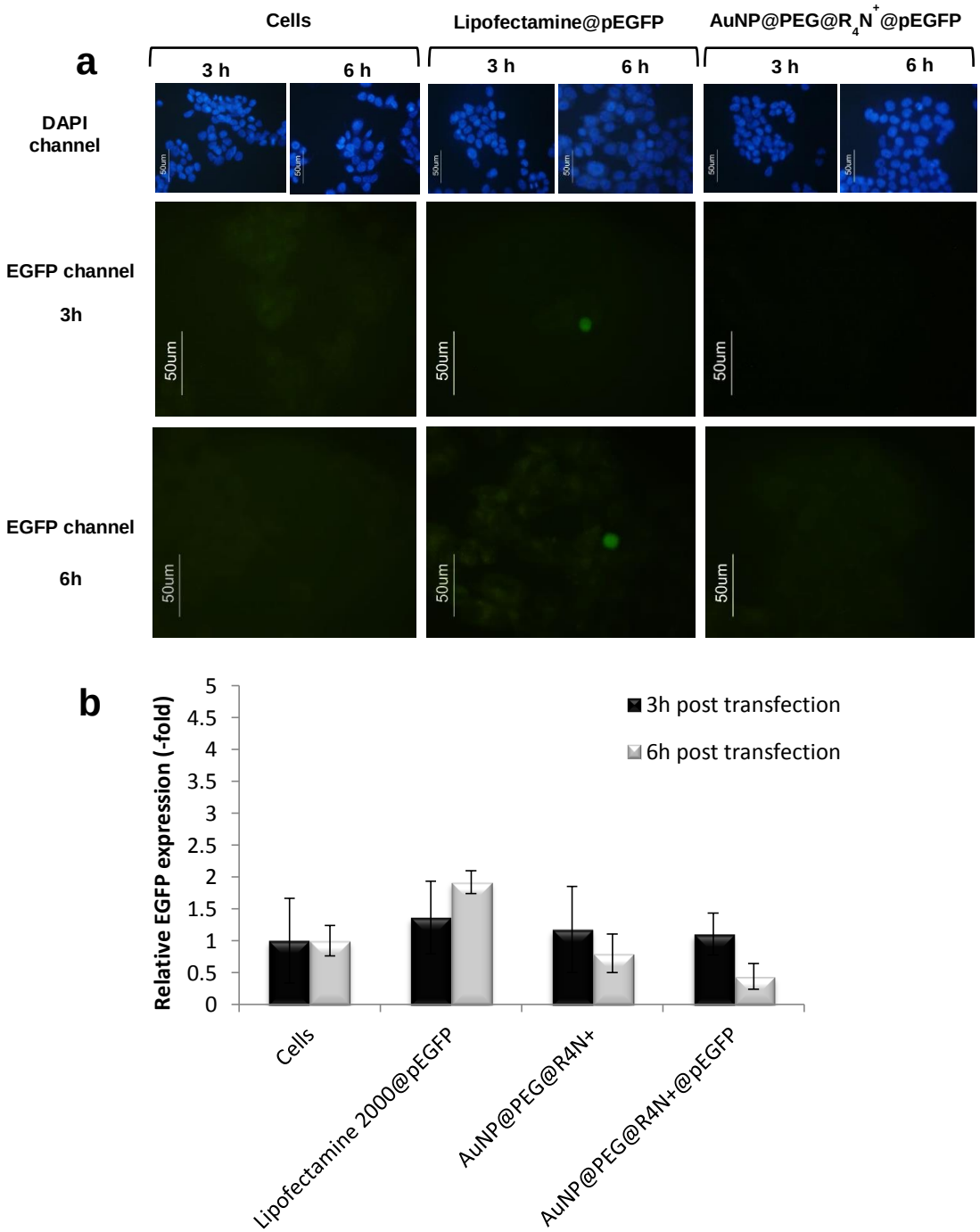

Figure 3.10 – (a) Images obtained by fluorescence microscopy (scale bar, 50 μm) of HCT-116 cells transfected with EGFP expression vector, using Lipofectamine 2000 and AuNP@PEG@R_4N^+@pEGFP, after 3h and 6h incubation. HCT-116 cells transfected using Lipofectamine 2000 shows a low level of EGFP expression, while with the AuNP@PEG@R_4N^+@pEGFP no expression was achieved; (b) Relative expression of EGFP was assessed by fluorescence spectroscopy, 3h and 6h after transfection HCT-116 cells transfected with 1 μg of the EGFP expression vector, using Lipofectamine 2000 and AuNP@PEG@R_4N^+@pEGFP. Not transfected cells and withAuNP@PEG@R_4N^+ were used as control.

Regarding the cells transfected with Lipofectamine 2000, the acquired images show some expression of EGFP as early as 3h and 6h post-transfection (see Figure 3.10a) , although a low level. These results are in agreement with those obtained by measuring fluorescence intensity of cell lysates (see Figure 3.10 b), in which an increase in relative EGFP expression of 0.3 and 0.91 was observed after 3h and 6h post transfection, respectively, compared to cells that were not transfected.

Concerning the cells transfected with AuNP@PEG@R_4N^+, the expression level remains unchanged when compared with the control cells, as shown by fluorescence microscopy (see Figure 3.10a) and by measuring the fluorescence of cells lysates (see Figure 3.10b). These results were not surprising because 3h and 6h post-transfection may not be enough time for the AuNPs complex to overcome the several barriers related to gene delivery vectors. Thus, the EGFP expression was assessed at 12h, 24h and 48h after transfection (see Figure 3.11).

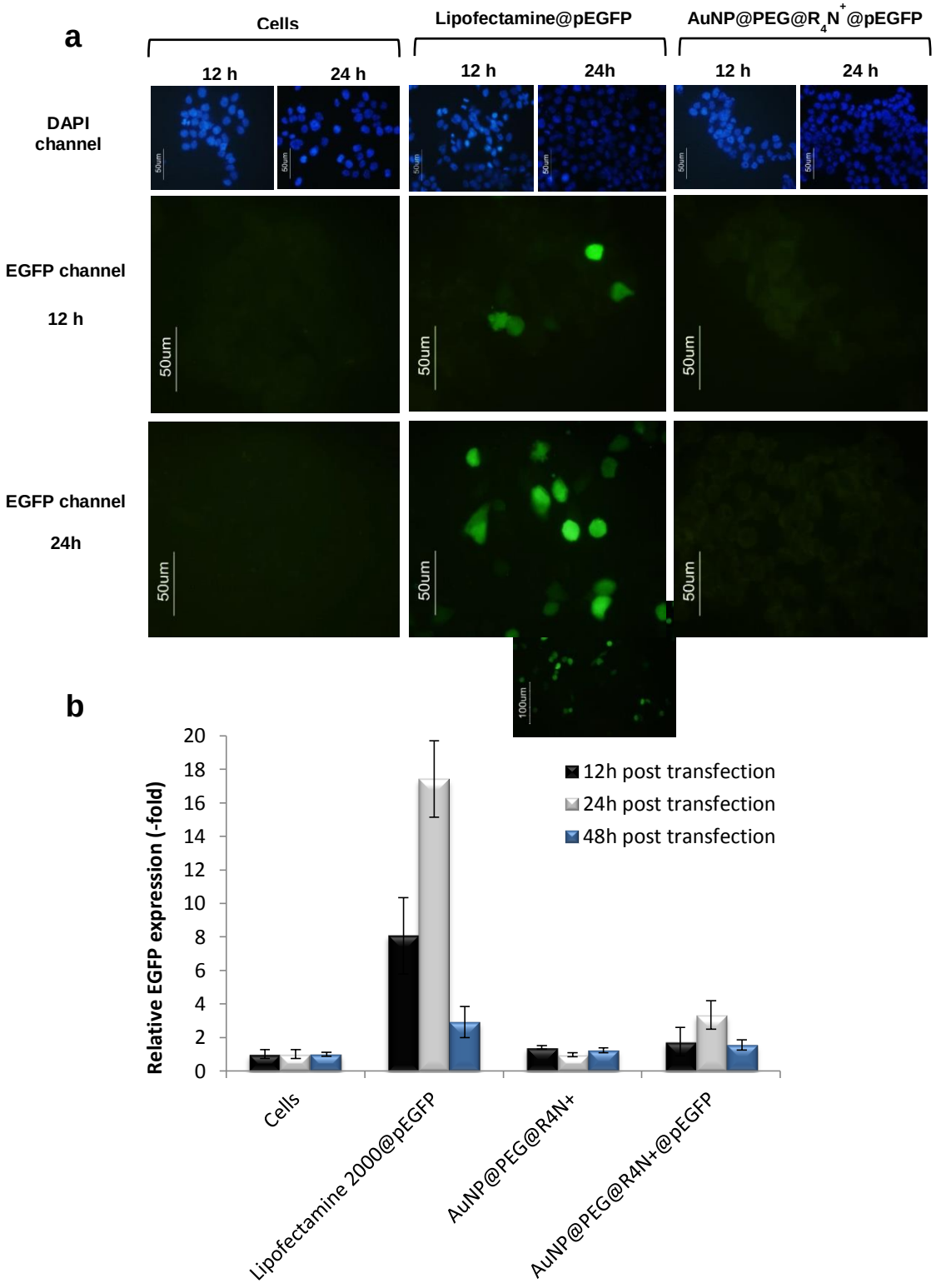

Figure 3.11 – (a) Images obtained by fluorescence microscopy (scale bar, 50 μm) of HCT-116 cells transfected with EGFP expression vector, using Lipofectamine 2000 and AuNP@PEG@R_4N^+@pEGFP, after 12h and 24h incubation; (b) Relative expression of EGFP was assessed by fluorescence spectroscopy, 12h, 24h and 48 h after transfection HCT-116 cells with 1 μg of the EGFP expression vector, using Lipofectamine 2000 and AuNP@PEG@R_4N^+@pEGFP. Not transfected cells and with AuNP@PEG@R_4N^+ were used as control.

Images acquired 12h and 24h after transfection of cells with the EGFP expression vector using Lipofectamine 2000 clearly showed efficient expression of the reporter gene (see Figure 3.11a). The images taken between 3 and 24h showed a trend, in which it was possible to confirm that the longer the incubation time, the higher the level of EGFP expression. This trend was also observed when fluorescence intensity of the cell lysates was acquired at 12h and 24h (Figure 3.11 b), in which relative expression of EGFP increased 4 fold between 6h and 12h, and 2 fold between 12h and 24h, i.e., between 3h and 24h it was observed a 17 fold increase. Curiously, the relative expression of EGFP decreases 48h post transfection but this can be explained by the cytotoxicity induced by Lipofectamine, which is known to cause toxicity to cells, and consequently the number of cells available to express EGFP decrease. Furthermore, this is a transient transfection in which plasmid does not replicate inside cells. Thus, plasmid gets diluted with cell division.

Regarding cells transfected with AuNP@PEG@R_4N^+@pEGFP, these showed negligible EGFP expression 12h post transfection, when compared with non-transfected cells and cells incubated with AuNP@PEG@R_4N^+. The relative expression of EGFP 24h after being transfected increased 3.34 times, whereas using Lipofectamine as gene delivery, the expression increased 17 times relatively to non-transfected cells. Both Lipofectamine and AuNP@PEG@R4N+@pEGFP carry the same amount of plasmid (1 μg), but Lipofectamine showed better transfection efficiency.

Although a low level of EGFP expression was achieved 24h after transfection with AuNP complexes, as shown by the fluorescence intensity of cell lysates (Figure 3.11b), the image corresponding to this assay in Figure 3.11a, did not clearly show an increase in the expression level relative to the image of control cells (non-transfected) acquired in the EGFP channel. These differences between both techniques may be due to their sensitivity. Due the barriers associated to non-viral gene delivery, there are several reasons that can explain this ineffectiveness of this AuNP-based gene delivery system. Thus, it was necessary to assess the internalization of AuNP complexes by cells, to better understand the system and further on the reasons for the low EGFP expression on transfected cells.

3.3.3 EVALUTION OF NANOCONJUGATE UPTAKE BY PCR

As mentioned above, a low level of EGFP expression was detected by fluorescence spectroscopy (relative EGFP expression increased ~3 times) which was not clearly observed in images acquired with fluorescence microscope, when transfection were performed with the AuNP-based formulation developed. Thus, to obtain more detailed information about cellular uptake of the AuNP-based formulation by cells, a PCR was performed with the total DNA extracted from non-transfected cells, from cells that had been incubated with AuNP@PEG@R_4N^+ (negative controls), from cells transfected with EGFP using Lipofectamine

2000 (positive control), and from cells incubated with AuNP@PEG@R_4N^+@pEGFP. The uptake was studied at different incubation times from 3h to 24h. As an internal PCR control the FTO gene (housekeeping gene) was used.

The resulting PCR products, originating using the extracted DNA as template were analyzed in a 1% agarose gel electrophoresis and are shown in Figure 3.12.

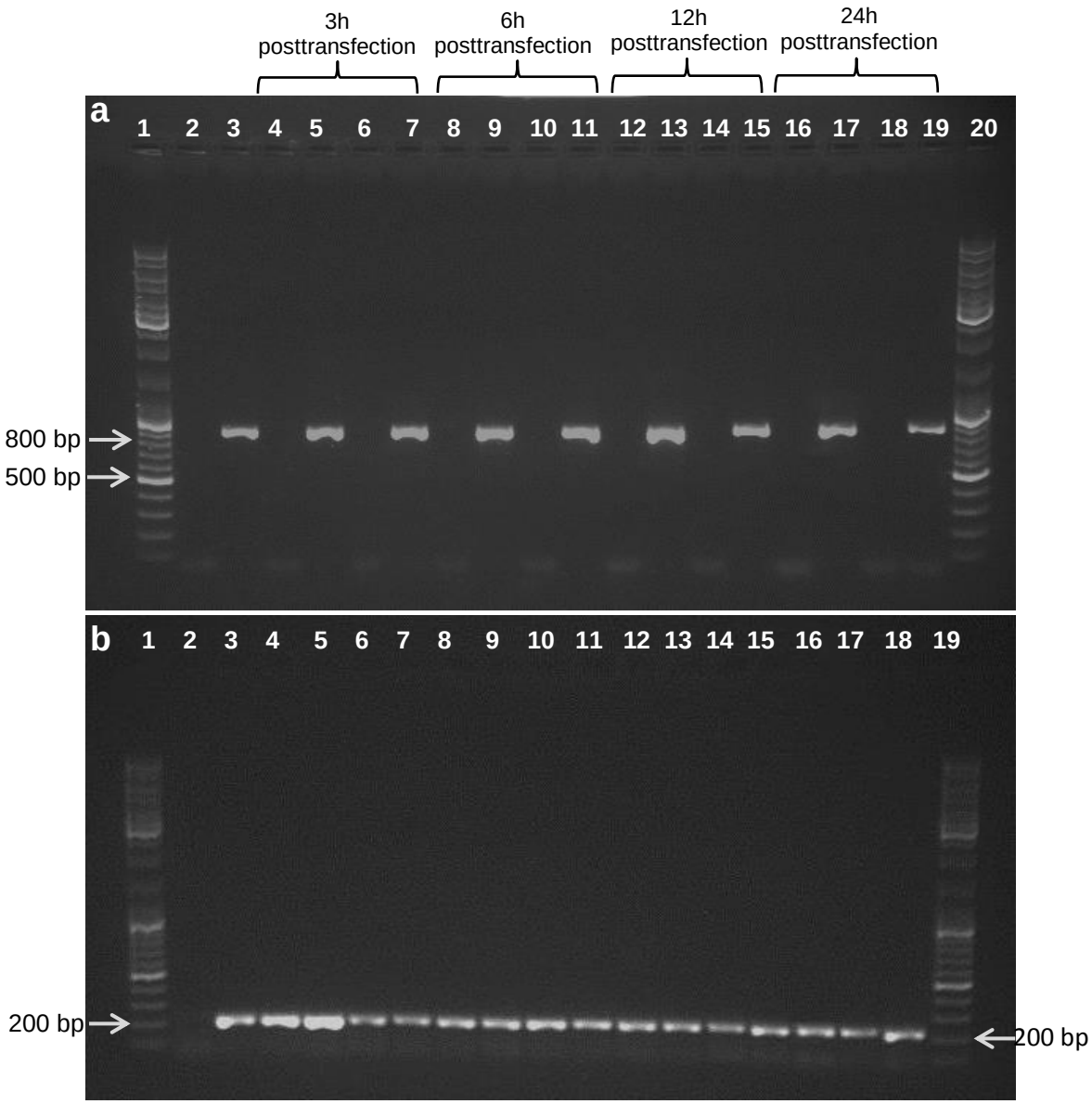

Figure 3.12 – Agarose gel electrophoresis (1%, 1x TAE, 60V 1h30) showing the amplification of EGFP gene using extracted DNA from transfected and non-transfected cells as template. (a) Lane 1 and 20 – ladder; lane 2 and 3 – control and EGFP plasmid amplified; lane 4 - 7 – 3h post transfection: cells, Lipofectamine@pEGFP, AuNP@PEG@R_4N^+, AuNP@PEG@R_4N^+@pEGFP, respectively; lane 8 -11 – 6h post transfection in same order described previously; lane 12 - 15 – 12h post transfection in same order described previously; lane 16 - 19 – 24h post transfection in same order described previously; (b) Amplification of FTO used as internal control. Lane 2 – control; Lane 3 – 6 – 3h post transfection: cells, Lipofectamine@pEGFP, AuNP@PEG@R_4N^+, AuNP@PEG@R_4N^+@pEGFP, respectively; lane 7 – 10 –

6h post transfection in same order described previously; lane 11 – 14 – 12h post 12h post transfection in same order described previously; lane 15 – 19 – 24h post transfection in same order described previously.

The cellular uptake of the EGFP expression vector, monitored by electrophoretic analysis in agarose gel of the PCR products using as template the DNA extracted from transfected cells, revealed AuNP complexes into the cells 3h after transfection. Once plasmid alone has no ability to enter the cells, due their negative charge which makes it impossible penetrate the cell membrane, it is possible to conclude that the AuNP-based formulation developed can enter into the cells. Moreover, the internalization of the EGFP vector was not only detected at 3h incubation, as well as in the range 3 – 24h. However, at 24h post transfection with AuNP@PEG@R_4N^+@pEGFP (lane 19), the decrease of the intensity of the band can be indicative that some plasmid has already been diluted. This may have occurred because this was a transient transfection in which the plasmid was not integrated into the genome. Thus, the plasmid was diluted when cells were divided. However, this is not quantitative PCR.

Once inside the cells, this delivery vector based on AuNPs overcomes one of the barriers in gene delivery, the cellular uptake. The ability of the nanocarrier to cross the cell membrane may be due to the effect of quaternary ammonium groups, which are responsible for the binding of plasmid to the nanocarrier but also, for establishing an electrostatic interaction with the cell membrane aiding in the internalization of the complex. Thus, in regard to cellular uptake, the delivery vector based on AuNPs was as efficient as Lipofectamine 2000.

With these results, it is possible to conclude that the size of the AuNP complexes (113.5 nm± 0.8) is not an issue in cellular uptake. Futhermore, it was reported that the use of larger particles, contribute to a major gene delivery in cytoplasm, due to its long residence time in this compartment, avoiding rapid lysosomal degradation (Rejman et al. 2004). With a size of 113.5 nm, the nanocarrier may be internalized through an endocytic process, since this process can be achieved with particles up to 150 nm.

Once internalized, the plasmid must overcome other barriers, such as endo-lysosomal entrapment and release, cytosolic sequestration, nuclear entry and metabolic degradation, which reduce the efficiency of gene transfer. Furthermore, it is estimated that at least 10^5 plasmids per cell are required in the extracellular compartment to ensure that a few DNA molecules are taken up into the nucleus (Lechardeur et al. 2005). Facing these problems, it was not surprising the results related to EGFP expression obtained by fluorescence microscopy and fluorescence spectroscopy, since the formulation developed was not functionalized with specific sequences or proteins/peptides that can help to overcome these barriers.

A studied achieved by Boyoglu et al., reported that AuNPs with sizes of 25 nm and 50 nm accumulated around the nucleus and remained in cytoplasm, after 1h incubation (Boyoglu et al. 2013). This barrier was overcome in the work developed by Kang et al., where they used 30 nm

AuNPs functionalized with nuclear localization signal (NLS) peptide, which are capable to bind specifically to nuclear membrane and must have facilitated a higher amount of AuNPs entry into the nucleus (Kang et al. 2010). Since it has been reported that quaternary ammonium groups have a possible proton-sponge effect, which could be responsible for endosome release of the entrapped nanocarrier (Yezhelyev et al. 2008), it was assumed that the inability of the AuNP-based formulation developed to successfully deliver the EGFP expression vector was not due to the inability of the nanocarrier to escape from the endosome. Furthermore, in images acquired with blue channel, where it was possible to see the nucleus stained with DAPI, it was observed some black spots over and around the nucleus, whereas in control cells and transfected with Lipofectamine 2000 these black spots were not observed (see section A3 in Appendix). This may suggest that some of the internalized AuNPs accumulated around the nucleus. What is not possible to conclude is whether the plasmid remains linked to the AuNP nanocarrier or if the pDNA was released from the AuNP complex.

Thus, it was considered that the two major challenges to successfully achieve the transfection were the trafficking of plasmid through the cytoplasm and nuclear entry. Moreover, it has been estimated that the half-life of naked plasmid DNA in the cytoplasm of cells ranges between 50 minutes and 5h. In a typical 24h transfection, assuming an average half-life of 3h, if the plasmid does not enter quickly into the nucleus, less than 0.4% of the input DNA would remain by 24h (Vaughan et al. 2006). However, at 24h post transfection it was still possible to confirm the presence of the plasmid in cells (see Figure 3.12a). This suggests that the plasmid was subjected to a protection which could be conferred, once again, by the quaternary ammonium groups.

The formulation based on the gold nanoparticles developed, as well as the plasmid, had limited access to the nucleus due to the restriction posed by the nuclear membrane. The mechanism of entry of the exogenous material into the nucleus is not yet fully understood. Furthermore, this process depends on the transfection technique and the delivery vectors. In the most commonly used transfection methods (e.g using lipoplexes), exogenous DNA gains access to the nucleus by traveling along microtubules or during cell division, since nuclear pores only allow the entry of molecules up to 30 nm (Lechardeur et al. 2005, Ondrej et al. 2007, Vaughan & Dean 2006).

Facing these issues, some hypothesis can explain why the plasmid DNA does not reach into the nucleus or just a low copie number can gain access to the nucleus. In case the plasmid does not dissociate from the nanocarrier, one explanation could concern the size of the nanocarrier. It is known that the nuclear pore complexes can be expanded up to 30 nm, so the nanocarrier could be too large to pass through nuclear pore complex. In case plasmid dissociated from the nanocarrier before entering the nucleus, plasmid entry into the nucleus becomes a challenge once in the absence of mitosis, the nuclear membrane remains largely

impermeable to plasmids (Vaughan et al. 2006). At last, if we consider that plasmid reach the nucleus, it is possible that the number of copies that can entry the nucleus is too low.

To conclude, it was shown that it was possible bind the EFGP expression vector to AuNPs conjugated with PEG and quaternary ammonium groups and overcome one of the barriers associated to non-viral gene delivery vectors - cell uptake.

3.4 TOXICITY ASSESSMENT OF AuNP-BASED FORMULATION

To characterize the system effects in terms of cell viability, a MTS assay was performed, which determines mitochondrial activity in living cells. As shown in Figure 3.13, no cell viability changes were detected up to 48h incubation for AuNP-based formulations. It would be expected some toxicity of the AuNP@PEG@R_4N^+@pEGFP, due to the quaternary ammoniums once these groups have strong interaction with the cell surface. However, no toxicity was observed which constitute a great advantage relative to Lipofectamine 2000.

However, significant decrease in cell viability in cells transfected with Lipofectamine was observed, which caused toxicity for 48 % of the cells. This can explain the low expression level of EGFP shown in Figure 3.11b, after 48h incubation of cells with Lipofectamine 2000. These types of cationic liposomes are already known to cause toxicity in cells and despite their great transfection efficiency, they cannot be deployed as non-viral gene delivery vectors for therapeutic approaches due their cytotoxicity.

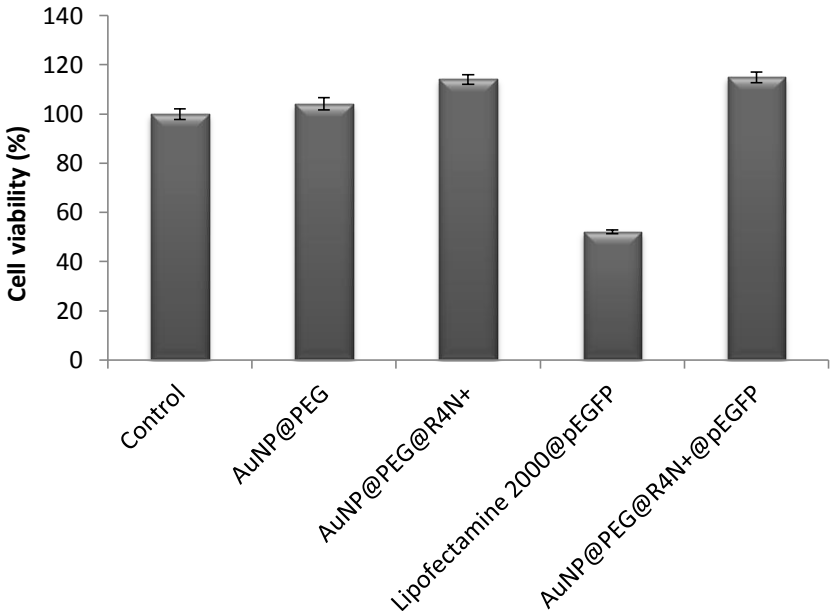

Figure 3.13 – Cell viability of HCT-116 cells after transfection with AuNPs-based formulations and Lipofectamine 2000, at 48 h of incubation. Negligible influence in cell viability is observed for all nanoconjugates tested when compared to untreated cells (control).

Although it has not been proved that the delivery vector developed can be used successfully as non-viral gene delivery vector due the ineffective transfection, this formulation based on AuNPs still had advantages when compared with cationic vectors, such as liposomes. Among these advantages are the lack of cytotoxicity, showed by the MTS assay, and the possibility of vectorization using antibodies, peptides, proteins that can help to overcome some of the barriers associated with gene delivery, whereas the gene delivery vectors, such as liposomes, make use of only non-specific mechanisms.

4. CONCLUSIONS AND FUTURE PERSPECTIVES

In this work it was proposed to design a non-viral gene delivery vector based in AuNPs capable to transfect plasmid DNA in a cancer cell line. The biocompatibility of the system was improved by attaching 4300 ± 114 PEG chains/AuNP. Furthermore, this group provides a moiety (carboxyl group) to bind quaternary ammonium groups, in which it was possible to link the EGFP expression vector via electrostatic interactions. The system was characterized by UV-vis spectroscopy, DLS and electrophoretic mobility. UV-vis spectroscopy allowed evaluation of the shift on SPR, which changes in function of the environment surrounding AuNPs. Thus, a SPR shift to a greater wavelength was indicative of functionalization and this was followed by the increase of the hydrodynamic diameter measured by DLS. Thus, it was observed a red-shift of the SPR from 521 to 533 nm since citrate-capped AuNPs to AuNP@PEG@R_4N^+@pEGFP. The cellular uptake is more challenging to larger nanoparticles, however the size of the formulation developed (AuNP@PEG@R4N+@pEGFP) determined by DLS, 113.5 ± 0.8 nm, did not appear to be a problem, since it could be internalized 3h post transfection.

The non-viral delivery vector developed that has some limitations that can be overcome with some optimizations, had shown great potential to be a viable alternative to the available methods, such as Lipofectamine. The results obtained for the cellular uptake, showed that the developed system is as effective as Lipofectamine, revealing a cellular uptake 3h post transfection. Furthermore, it was possible to conclude that up to 24h there was still DNA present within the cell and it was not totally degraded, which indicates that this is subject to some kind of protection.

The methods used to assess EGFP expression, fluorescence microscopy and spectroscopy, revealed a low expression EGFP expression in cells transfected with AuNP-based formulation 24h post transfection. This can be probably due to the inability of the plasmid enter the nucleus or the low copy number of plasmid that can reach the nucleus. Since EGFP expression was not successfully achieved, some optimizations of the system and/or transfection procedure are needed. Once it has been proposed that the major barrier is the entry into the nucleus, it is proposed a new design of the delivery system by functionalization with nuclear localization signal peptides that are known to facilitate nuclear entry. Another method that can be used to promote EGFP expression is inducing this with IPTG. Alternatively, the intracellular trafficking of the formulation and pDNA could be followed by recording TEM images, in order to understand the principal limitation of the formulation once inside the cells. If the expression was achieved, this could be enhanced through vectorization of the formulation with e.g. EGFR (epidermal growth factor receptor) antibody. EGFR is a transmembrane tyrosine kinase receptor that is overexpressed in multiple cancer types, especially colorectal cancer, and appears to promote solid tumor growth (Krasinskas 2011). Once successfully achieved EGFP expression, quantitative real-time PCR must be performed to evaluate expression of EGFP.

Regarding to cytotoxicity, 48h after exposure of HCT-116 cells to both AuNP-based formulation and Lipofectamine 2000, significant differences were observed. Lipofectamine 2000 caused toxicity to 50 % of the cells, while AuNP-based formulation showed no toxicity to cells. In a future work, it would be desirable determine the cell viability in shorter incubation times.

At last, facing the problems inherent to intracellular trafficking of non-viral delivery vectors, is suitable to say that formulation developed here is more suitable to use in mechanisms that do not involve the nuclear entry, such as siRNA or antisense oligonucleotides.

5. REFERENCES

Al-Dosari MS, Gao X. 2009. Nonviral gene delivery: principle, limitations, and recent progress. *AAPS J.* 11(4):671–81

Alkilany AM, Murphy CJ. 2010. Toxicity and cellular uptake of gold nanoparticles: what we have learned so far? *J. Nanopart. Res.* 12(7):2313–33

Baptista P, Doria G, Henriques D, Pereira E, Franco R. 2005. Colorimetric detection of eukaryotic gene expression with DNA-derivatized gold nanoparticles. *J. Biotechnol.* 119(2):111–17

Baptista P. 2009. Cancer Nanotechnology - Prospects for Cancer Diagnostics and Therapy. Current Cancer Therapy Reviews. 5(2):80-88

Boisselier E, Astruc D. 2009. Gold nanoparticles in nanomedicine: preparations, imaging, diagnostics, therapies and toxicity. *Chem. Soc. Rev.* 38(6):1759–82

Boyoglu C, He Q, Willing G, Boyoglu-barnum S, Dennis VA, et al. 2013. Microscopic Studies of Various Sizes of Gold Nanoparticles and Their Cellular Localizations. *ISRN Nanotechnol.* 2013:1–13

Brust M, Walker M, Bethell D, Schiffrin DJ, Whyman R. 1994. Synthesis of Thiol-derivatised Gold Nanoparticles in. *J. Chem. Soc., Chem. Commun*, pp. 801–2

Cevher E, Sezer A, Çağlar E. 2012. Gene delivery systems: Recent progress in viral and non-viral therapy. *Recent Adv. Nov. Drug Carr. Syst.*, pp. 437–70

Chithrani BD, Ghazani A a, Chan WCW. 2006. Determining the size and shape dependence of gold nanoparticle uptake into mammalian cells. *Nano Lett.* 6(4):662–68

Chou LYT, Ming K, Chan WCW. 2011. Strategies for the intracellular delivery of nanoparticles. *Chem. Soc. Rev.* 40(1):233–45

Conde J, Ambrosone A, Sanz V, Hernandez Y, Marchesano V, et al. 2012a. Design of Multifunctional Gold Nanoparticles for In Vitro and In Vitro Gene Silencing. *ACS Nano*. 6(9):8316–24

Conde J, Dias JT, Grazú V, Moros M, Baptista P V, de la Fuente JM. 2014a. Revisiting 30 years of biofunctionalization and surface chemistry of inorganic nanoparticles for nanomedicine. *Front. Chem.* 2:1–27

Conde J, Doria G, Baptista P. 2012b. Noble metal nanoparticles applications in cancer. *J. Drug Deliv.* 2012:751075

Conde J, Larguinho M, Cordeiro A, Raposo LR, Costa PM, et al. 2014b. Gold-nanobeacons for gene therapy: evaluation of genotoxicity, cell toxicity and proteome profiling analysis. *Nanotoxicology*. 8(5):521–32

Connor EE, Mwamuka J, Gole A, Murphy CJ, Wyatt MD. 2005. Gold nanoparticles are taken up by human cells but do not cause acute cytotoxicity. *Small*. 1(3):325–27

Cotrim AP, Baum BJ. 2008. Gene therapy: some history, applications, problems, and prospects. *Toxicol. Pathol.* 36(1):97–103

Delong RK, Reynolds CM, Malcolm Y, Schaeffer A, Severs T, Wanekaya A. 2010. Functionalized gold nanoparticles for the binding, stabilization, and delivery of therapeutic DNA, RNA, and other biological macromolecules. *Nanotechnol. Sci. Appl.* 3:53–63

Dreaden EC, Alkilany AM, Huang X, Murphy CJ, El-Sayed M a. 2012. The golden age: gold nanoparticles for biomedicine. *Chem. Soc. Rev.* 41(7):2740–79

Dreaden EC, Mackey M a, Huang X, Kang B, El-Sayed M a. 2011. Beating cancer in multiple ways using nanogold. *Chem. Soc. Rev.* 40(7):3391–3404

Elsabahy M, Nazarali A, Foldvari M. 2011. Non-viral nucleic acid delivery: key challenges and future directions. *Curr. Drug Deliv.* 8(3):235–44

El-Sayed A, Harashima H. 2013. Endocytosis of gene delivery vectors: from clathrin-dependent to lipid raft-mediated endocytosis. *Mol. Ther.* 21(6):1118–30

El-Sayed M a. 2001. Some interesting properties of metals confined in time and nanometer space of different shapes. *Acc. Chem. Res.* 34(4):257–64

Eustis S, el-Sayed M a. 2006. Why gold nanoparticles are more precious than pretty gold: noble metal surface plasmon resonance and its enhancement of the radiative and nonradiative properties of nanocrystals of different shapes. *Chem. Soc. Rev.* 35(3):209–17

Fakruddin M, Hossain Z, Afroz H. 2012. Prospects and applications of nanobiotechnology: a medical perspective. *J. Nanobiotechnology*. 10(1):31

Faraday M. 1857. Experimental relations of gold (and other metals) to light. *Philos. Trans. R. Soc. London*. 147:145–81

Frens G. 1973. Controlled Nucleation for the Regulation of the Particle Size in Monodisperse Gold Suspensions. *Nat. Phys. Sci.* 241:20–22

Gascón AR, Pozo-rodríguez A, Solinís MÁ. 2013. Non-Viral Delivery Systems in Gene Therapy. In *Gene Therapy - Tools and Potential Applications*, pp. 3–34

GLOBOCAN 2012. http://globocan.iarc.fr/ (accessed in April, 2014)

Ghosh PS, Kim C, Han G, Forbes NS, Rotello VM. 2008. Efficient Gene Delivery Vectors by Tuning the Surface Charge Density of. *ACS Nano*. 2(11):2213–18

Haiss W, Thanh NTK, Aveyard J, Fernig DG. 2007. Determination of size and concentration of gold nanoparticles from UV-vis spectra. *Anal. Chem.* 79(11):4215–21

Han G, Martin CT, Rotello VM. 2006. Stability of gold nanoparticle-bound DNA toward biological, physical, and chemical agents. *Chem. Biol. Drug Des.* 67(1):78–82

Hanahan D, Weinberg R a. 2011. Hallmarks of cancer: the next generation. *Cell*. 144(5):646–74

Huang X, Jain PK, El-Sayed IH, El-Sayed M a. 2007. Gold nanoparticles: interesting optical properties and recent applications in cancer diagnostics and therapy. *Nanomedicine*. 2(5):681–93

Iris Biotech GMBH, Reagents. http://www.iris-biotech.de/ (accessed in August, 2014).

Jain KK. 2008. Nanomedicine: application of nanobiotechnology in medical practice. *Med. Princ. Pract.* 17(2):89–101

Jones CH, Chen C-K, Ravikrishnan A, Rane S, Pfeifer B a. 2013. Overcoming nonviral gene delivery barriers: perspective and future. *Mol. Pharm.* 10(11):4082–98

Kaliberov S, Buchsbaum D. 2012. Cancer Treatment with Gene Therapy and Radiation Therapy. *Adv Cancer Res*. 115:221–63

Kang B, Mackey M a, El-Sayed M a. 2010. Nuclear targeting of gold nanoparticles in cancer cells induces DNA damage, causing cytokinesis arrest and apoptosis. *J. Am. Chem. Soc.* 132(5):1517–19

Khalel RR, Parvez N, Yadav S, Hwisa N. 2010. Nanotechnology in Cancer Therapy : A Review. *J. Chem. Pharm. Res.* 2(5):161–68

Khalil IA, Kogure K, Akita H, Harashima H. 2006. Uptake Pathways and Subsequent Intracellular Trafficking in Nonviral Gene Delivery. . 58(1):32–45

Khan MS, Vishakante GD, Siddaramaiah H. 2013. Gold nanoparticles: a paradigm shift in biomedical applications. *Adv. Colloid Interface Sci.* 199-200:44–58

Krasinskas AM. 2011. EGFR Signaling in Colorectal Carcinoma. *Patholog. Res. Int.* 2011:1–6

Ladj R, Bitar a., Eissa M, Mugnier Y, Le Dantec R, et al. 2013. Individual inorganic nanoparticles: preparation, functionalization and in vitro biomedical diagnostic applications. *J. Mater. Chem. B*. 1(10):1381

Lechardeur D, Verkman a S, Lukacs GL. 2005. Intracellular routing of plasmid DNA during non-viral gene transfer. *Adv. Drug Deliv. Rev.* 57(5):755–67

Lee C, Meisel D. 1982. Adsorption and Surface-Enhanced Raman of Dyes on Silver and Gold Sols'. *J. Phys. Chem.* 83(17):3391–95

Liang A, Liu Q, Wen G, Jiang Z. 2012. The surface-plasmon-resonance effect of nanogold/silver and its analytical applications. *Trends Anal. Chem.* 37:32–47

Liang W, Lam JKW. 2012. Endosomal Escape Pathways for Non-Viral Nucleic Acid Delivery Systems. In *Molecular Regulation of Endocytosis*, pp. 429–56

Liu C, Zhang N. 2011. Nanoparticles in Gene Therapy: Principles, Prospects, and Challenges. In *Progress in Molecular Biology and Translational Science*, Vol. 104, pp. 509–62. Elsevier Inc. 1st ed.

Liu Y, Miyoshi H, Nakamura M. 2007. Nanomedicine for drug delivery and imaging: a promising avenue for cancer therapy and diagnosis using targeted functional nanoparticles. *Int. J. cancer.* 120(12):2527–37

Llevot A, Astruc D. 2012. Applications of vectorized gold nanoparticles to the diagnosis and therapy of cancer. *Chem. Soc. Rev.* 41(1):242–57

McIntosh CM, Esposito E a, Boal a K, Simard JM, Martin CT, Rotello VM. 2001. Inhibition of DNA transcription using cationic mixed monolayer protected gold clusters. *J. Am. Chem. Soc.* 123(31):7626–29

Medina-Kauwe LK, Xie J, Hamm-Alvarez S. 2005. Intracellular trafficking of nonviral vectors. *Gene Ther.* 12(24):1734–51

Nazir S, Hussain T, Ayub A, Rashid U, MacRobert AJ. 2014. Nanomaterials in combating cancer: therapeutic applications and developments. *Nanomedicine*. 10:19–34

Niemeyer CM, Mirkin CA. 2004. *Nanobiotechnology: Concepts, Applications and Perspectives*

Ondrej V, Lukásová E, Falk M, Kozubek S. 2007. The role of actin and microtubule networks in plasmid DNA intracellular trafficking. *Acta Biochim. Pol.* 54(3):657–63

Ozluer C, Kara HES. 2014. In vitro DNA binding studies of anticancer drug idarubicin using spectroscopic techniques. *J. Photochem. Photobiol. B.* 138:36–42

Patil SD, Rhodes DG, Burgess DJ. 2005. DNA-based therapeutics and DNA delivery systems: a comprehensive review. *AAPS J.* 7(1):E61–77

Peer D, Karp JM, Hong S, Farokhzad OC, Margalit R, Langer R. 2007. Nanocarriers as an emerging platform for cancer therapy. *Nat. Nanotechnol.* 2(12):751–60

Prasad SC, Roy I. 2008. Nucleic acid based therapeutic molecules. *CRIPS*. 9:49–55

Pushpendra S, Arvind P, Anil B. 2012. Nucleic Acids as Therapeutics. In *From Nucleic Acids Sequences to Molecular Medicine*, eds. VA Erdmann, J Barciszewski, pp. 19–46. Berlin, Heidelberg: Springer Berlin Heidelberg

Rejman J, Oberle V, Zuhorn IS, Hoekstra D. 2004. Size-dependent internalization of particles via the pathways of clathrin- and caveolae-mediated endocytosis. *Biochem. J.* 377:159–69

Sandhu KK, McIntosh CM, Simard JM, Smith SW, Rotello VM. 2002. Gold nanoparticle-mediated transfection of mammalian cells. *Bioconjug. Chem.* 13(1):3–6

Society AC. 2014. Cancer Facts & Figures 2014. *Atlanta Am. Cancer Soc.*

Sperling R a, Parak WJ. 2010. Surface modification, functionalization and bioconjugation of colloidal inorganic nanoparticles. *Philos. Trans. R. Soc.* 368(1915):1333–83

Sperling RA, Gil PR, Zhang F, Zanella M, Parak WJ. 2008. Biological applications of gold nanoparticles. *Chem. Soc. Rev.* 37:1896–1908

Tiwari P, Vig K, Dennis V, Singh S. 2011. Functionalized Gold Nanoparticles and Their Biomedical Applications. *Nanomaterials*. 1(1):31–63

Turkevich J, Garton G, Stevenson PC. 1954. The color of colloidal gold. *J. Colloid. Sci.* 9:26–35

Turner M, Golovko VB, Vaughan OPH, Abdulkin P, Berenguer-Murcia A, et al. 2008. Selective oxidation with dioxygen by gold nanoparticle catalysts derived from 55-atom clusters. *Nature*. 454(7207):981–84

Varkouhi AK, Scholte M, Storm G, Haisma HJ. 2011. Endosomal escape pathways for delivery of biologicals. *J. Control. Release*. 151(3):220–28

Vaughan EE, Dean D a. 2006. Intracellular trafficking of plasmids during transfection is mediated by microtubules. *Mol. Ther.* 13(2):422–28

Vaughan EE, DeGiulio J V, Dean D a. 2006. Intracellular trafficking of plasmids for gene therapy: mechanisms of cytoplasmic movement and nuclear import. *Curr. Gene Ther.* 6(6):671–81

Villiers C, Freitas H, Couderc R, Villiers M-B, Marche P. 2010. Analysis of the toxicity of gold nano particles on the immune system: effect on dendritic cell functions. *J. Nanopart. Res.* 12(1):55–60

Wang W, Li W, Ma N, Steinhoff G. 2013. Non-viral gene delivery methods. *Curr. Pharm. Biotechnol.* 14(1):46–60

Yezhelyev M V, Qi L, O'Regan RM, Nie S, Gao X. 2008. Proton-sponge coated quantum dots for siRNA delivery and intracellular imaging. *J. Am. Chem. Soc.* 130(28):9006–12

6. APPENDIX

A1. pVisionGFP-N Vector

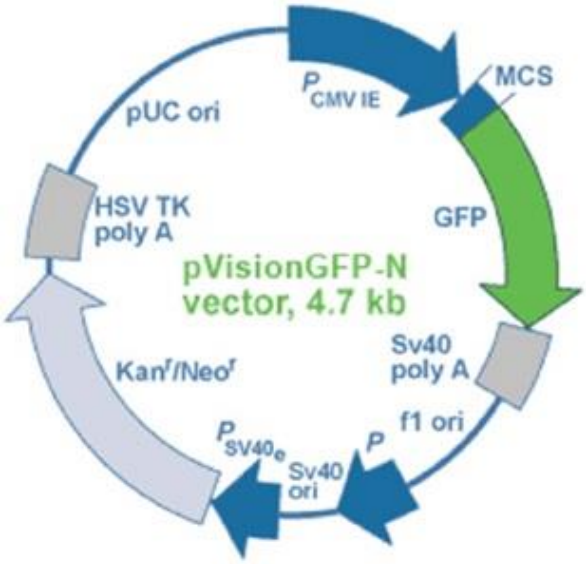

Figure A1 - Schematic representation of pVisionGFP-N Vector.

A2. LYSIS SOLUTIONS TO PLASMID EXTRACTION

Lysis I

50 mM Glucose

25 mM Tris-HCl pH 8

10mM EDTA pH 8

Sterilised by autoclaving at 110 ºC for 25 minutes and stored at 4ºC.

Lysis II

200 mM NaOH

1% (w/v) SDS freshly prepared (room temperature).

Lysis III

3M sodium acetate (The pH was adjusted to 4.8 with glacial acetic acid)

Stored at 4ºC and kept in ice during use.

A3. IMAGES ACQUIRED IN DAPI CHANNEL 24H POST TRANSFECTION

Cells
24 h post transfection

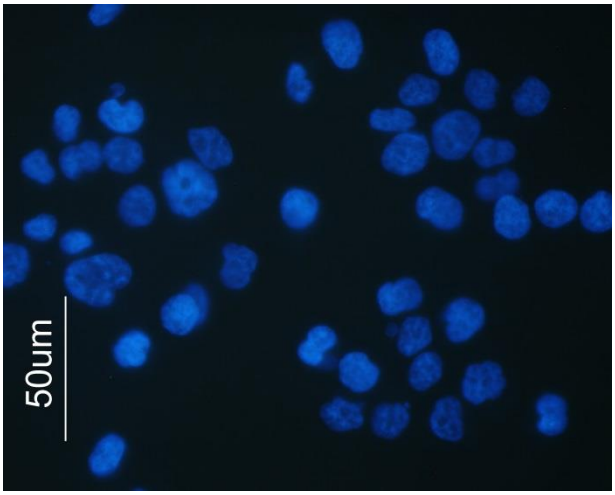

Lipofectamine
24 h post transfection

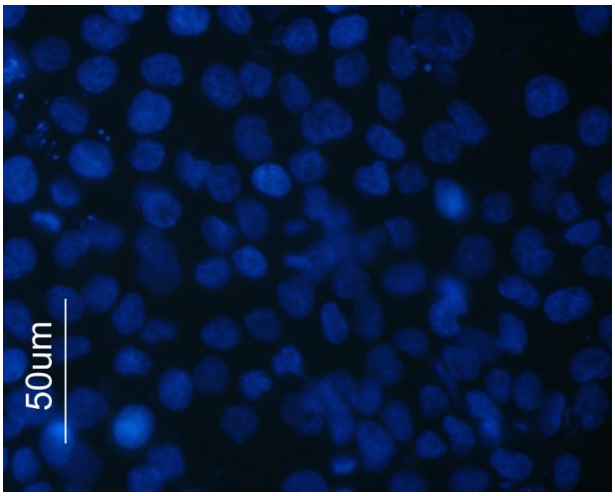

AuNP@PEG@R4N+@pEGFP
24 h post transfection